DISCUSSION

This study shows the positive correlation between the Val^{247} β_2GPI allele and anti-β_2GPI antibody production in a Japanese population, confirming the correlation observed in a British Caucasian population in our previous report (15). A positive correlation between the Val^{247} allele and the presence of anti-β_2GPI antibodies was also reported in Asian American (26) and Mexican patients (27). However, this correlation was not observed in other American populations (26) or in patients with thrombosis or pregnancy complications in the UK (28). This discrepancy may be the result of the difference in the frequency of the Val^{247} allele among races, or the difference in the background of investigated patients. Another possibility is that the relationship between the Val^{247} allele and thrombosis in Caucasians may be controversial due to underpowered studies or to differences in the procedure used to detect anti-β_2GPI antibodies. Methods for the detection of anti-β_2GPI antibodies differ among laboratories. For example, cardiolipin-coated plates or oxygenated plates are used in some methods, whereas unoxygenated plates are used in others. In addition, bovine β_2GPI is used instead of human β_2GPI in some assays. The antibodies used for standardization also differ, although monoclonal antibodies such as EY2C9 and HCAL (29) have been proposed as international standards of calibration materials.

β_2GPI is a major target antigen for aCL, and, according to our previous investigation, B cell epitopes reside in domain IV and are considered to be cryptic and to appear only when β_2GPI interacts with negatively charged surfaces such as cardiolipin, phosphatidylserine, or polyoxygenated polystyrene surface (7), although other studies indicate that the B cell epitopes are located on domain I (13) or domain V (14). According to another interpretation for the specificity of aCL, increment of the local antigen density on the negatively charged surface also contributes to anti-β_2GPI detection in ELISA (8,30). Studies on the crystal structure of human β_2GPI revealed that the lysine-rich site and an extended C-terminal loop region on domain V are crucial for phospholipid binding. Position 247 is located at the N-terminal side of domain V, and, around this position, Lys^{242}, Ala^{243}, and Ser^{244} were suggested to play a role in the interaction between domains IV and V (9,23,31).

Although the Val/Leu^{247} polymorphism may not be very critical for the autoantibody binding, the amino acid substitution at this point was revealed to affect the affinity of monoclonal aCL established from patients with APS and that of purified IgG from patients positive for β_2GPI-dependent aCL. We conformationally optimized to domain V and the domain IV–V complex of β_2GPI variants at position 247, referring the crystal structure of β_2GPI. IgG aCL was screened using the standardized aCL ELISA, in which both the Leu^{247} and the Val^{247} allele of β_2GPI are contained as antigen. Although biochemical characteristics and structure are similar between valine and leucine, the replacement of Leu^{247} by Val^{247} leads to a significant alteration in the tertiary structure of domain V and/or the domain IV–V interaction (Figure 4). It is likely that the structural alteration affects the affinity between anti-β_2GPI autoantibodies and the epitope(s) present on its molecule. One explanation for this phenomenon is that this β_2GPI polymorphism affects the electrostatic interaction between domain IV and domain V or the protein–protein interaction, resulting in differences in the accessibility of the recognition site by the autoantibodies, or the local density of β_2GPI.

Another possible explanation of the correlation between the Val/Leu^{247} polymorphism of β_2GPI and anti-β_2GPI antibodies is T cell reactivity. Ito et al (32) investigated T cell epitopes of patients with anti-β_2GPI autoantibodies by stimulating patients' PBMCs with a peptide library that covers the β_2GPI sequence. Four of 7 established CD4+ T cell clones reacted to peptide fragments that include amino acid position 244–264, then position 247 is included among the candidate epitopes. Arai et al (33) found preferred recognition of peptide position 276–290 by T cell clones from patients with APS. They also found high reactivity to peptide 247–261 in one patient. We speculate that a small alteration in the conformation arising from the valine/leucine substitution at position 247 may affect the susceptibility to generate autoreactive T cell clones in patients with APS.

Our results in this study indicate that the Val/Leu^{247} polymorphism affects the antigenicity of β_2GPI for anti-β_2GPI autoantibodies, and that the Val^{247} allele can be a risk factor for having autoantibodies against this molecule. Therefore, the Val/Leu^{247} variation of β_2GPI may be crucial for autoimmune reactivity against β_2GPI. We further show the significance of the Val/Leu^{247} polymorphism of β_2GPI in the strength of the binding between β_2GPI and anti-β_2GPI autoantibodies. The significance of antigen polymorphisms in the production of autoantibodies or in the development of autoimmune diseases is not well understood. To our knowledge, this report is the first to present a genetic polymorphism of

autoantigen directly affecting its interaction with autoantibodies.

REFERENCES

1. Hughes GR. The antiphospholipid syndrome: ten years on. Lancet 1993;342:341–4.
2. Hughes GR, Harris EN, Gharavi AE. The anticardiolipin syndrome. J Rheumatol 1986;13:486–9.
3. Harris EN, Gharavi AE, Hughes GR. Anti-phospholipid antibodies. Clin Rheum Dis 1985;11:591–609.
4. Galli M, Comfurius P, Maassen C, Hemker HC, de Baets MH, van Breda-Vriesman PJ, et al. Anticardiolipin antibodies (ACA) directed not to cardiolipin but to a plasma protein cofactor. Lancet 1990;335:1544–7.
5. McNeil HP, Simpson RJ, Chesterman CN, Krilis SA. Anti-phospholipid antibodies are directed against a complex antigen that includes a lipid-binding inhibitor of coagulation: β_2-glycoprotein I (apolipoprotein H). Proc Natl Acad Sci U S A 1990;87:4120–4.
6. Matsuura E, Igarashi Y, Fujimoto M, Ichikawa K, Koike T. Anticardiolipin cofactor(s) and differential diagnosis of autoimmune disease. Lancet 1990;336:177–8.
7. Matsuura E, Igarashi Y, Yasuda T, Triplett DA, Koike T. Anticardiolipin antibodies recognize β_2-glycoprotein I structure altered by interacting with an oxygen modified solid phase surface. J Exp Med 1994;179:457–62.
8. Roubey RA, Eisenberg RA, Harper MF, Winfield JB. "Anticardiolipin" autoantibodies recognize β_2-glycoprotein I in the absence of phospholipid: importance of Ag density and bivalent binding. J Immunol 1995;154:954–60.
9. Schwarzenbacher R, Zeth K, Diederichs K, Gries A, Kostner GM, Laggner P, et al. Crystal structure of human β_2-glycoprotein I: implications for phospholipid binding and the antiphospholipid syndrome. EMBO J 1999;18:6228–39.
10. Sanghera DK, Kristensen T, Hamman RF, Kamboh MI. Molecular basis of the apolipoprotein H (β_2-glycoprotein I) protein polymorphism. Hum Genet 1997;100:57–62.
11. Yasuda S, Tsutsumi A, Chiba H, Yanai H, Miyoshi Y, Takeuchi R, et al. β_2-glycoprotein I deficiency: prevalence, genetic background and effects on plasma lipoprotein metabolism and hemostasis. Atherosclerosis 2000;152:337–46.
12. Igarashi M, Matsuura E, Igarashi Y, Nagae H, Ichikawa K, Triplett DA, et al. Human β_2-glycoprotein I as an anticardiolipin cofactor determined using mutants expressed by a baculovirus system. Blood 1996;87:3262–70.
13. Iverson GM, Victoria EJ, Marquis DM. Anti-β_2 glycoprotein I (β_2GPI) autoantibodies recognize an epitope on the first domain of β_2GPI. Proc Natl Acad Sci U S A 1998;95:15542–6.
14. Wang MX, Kandiah DA, Ichikawa K, Khamashta M, Hughes G, Koike T, et al. Epitope specificity of monoclonal anti-β_2-glycoprotein I antibodies derived from patients with the antiphospholipid syndrome. J Immunol 1995;155:1629–36.
15. Atsumi T, Tsutsumi A, Amengual O, Khamashta MA, Hughes GR, Miyoshi Y, et al. Correlation between β_2-glycoprotein I valine/leucine^{247} polymorphism and anti-β_2-glycoprotein I antibodies in patients with primary antiphospholipid syndrome. Rheumatology (Oxford) 1999;38:721–3.
16. Matsuura E, Igarashi Y, Fujimoto M, Ichikawa K, Suzuki T, Sumida T, et al. Heterogeneity of anticardiolipin antibodies defined by the anticardiolipin cofactor. J Immunol 1992;148:3885–91.
17. Atsumi T, Ieko M, Bertolaccini ML, Ichikawa K, Tsutsumi A, Matsuura E, et al. Association of autoantibodies against the phosphatidylserine–prothrombin complex with manifestations of the antiphospholipid syndrome and with the presence of lupus anticoagulant. Arthritis Rheum 2000;43:1982–93.
18. Wilson WA, Gharavi AE, Koike T, Lockshin MD, Branch DW, Piette JC, et al. International consensus statement on preliminary classification criteria for definite antiphospholipid syndrome: report of an international workshop. Arthritis Rheum 1999;42:1309–11.
19. Tan EM, Cohen AS, Fries JF, Masi AT, McShane DJ, Rothfield NF, et al. The 1982 revised criteria for the classification of systemic lupus erythematosus. Arthritis Rheum 1982;25:1271–7.
20. Ichikawa K, Khamashta MA, Koike T, Matsuura E, Hughes GR. β_2-glycoprotein I reactivity of monoclonal anticardiolipin antibodies from patients with antiphospholipid syndrome. Arthritis Rheum 1994;37:1453–61.
21. Matsuura E, Igarashi M, Igarashi Y, Nagae H, Ichikawa K, Yasuda T, et al. Molecular definition of human β_2-glycoprotein I (β_2-GPI) by cDNA cloning and inter-species differences of β_2-GPI in alternation of anticardiolipin binding. Int Immunol 1991;3:1217–21.
22. Matsuura E, Igarashi Y, Yasuda T, Triplett DA, Koike T. Anticardiolipin antibodies recognize β_2-glycoprotein I structure altered by interacting with an oxygen modified solid phase surface. J Exp Med 1994;179:457–62.
23. Bouma B, de Groot PG, van den Elsen JM, Ravelli RB, Schouten A, Simmelink MJ, et al. Adhesion mechanism of human β_2-glycoprotein I to phospholipids based on its crystal structure. EMBO J 1999;18:5166–74.
24. Brooks BR, Bruccoleri RE, Olafson BD, States DJ. CHARMm: a program for macromolecular energy, minimization, and dynamics calculations. J Comput Chem 1983;4:187–217.
25. Carlson W, Karplus M, Haber E. Construction of a model for the three-dimensional structure of human renal renin. Hypertension 1985;7:13–26.
26. Hirose N, Williams R, Alberts AR, Furie RA, Chartash EK, Jain RI, et al. A role for the polymorphism at position 247 of the β_2-glycoprotein I gene in the generation of anti-β_2-glycoprotein I antibodies in the antiphospholipid syndrome. Arthritis Rheum 1999;42:1655–61.
27. Prieto GA, Cabral AR, Zapata-Zuñiga M, Simón AJ, Villa AR, Alarcon-Segovia D, et al. Valine/valine genotype at position 247 of the β_2-glycoprotein I gene in Mexican patients with primary antiphospholipid syndrome: association with anti-β_2-glycoprotein I antibodies. Arthritis Rheum 2003;48:471–4.
28. Camilleri RS, Mackie IJ, Humphries SE, Machin SJ, Cohen H. Lack of association of β_2-glycoprotein I polymorphisms Val247Leu and Trp316Ser with antiphospholipid antibodies in patients with thrombosis and pregnancy complications. Br J Haematol 2003;120:1066–72.
29. Ichikawa K, Tsutsumi A, Atsumi T, Matsuura E, Kobayashi S, Hughes GR, et al. A chimeric antibody with the human γ1 constant region as a putative standard for assays to detect IgG β_2-glycoprotein I–dependent anticardiolipin and anti-β_2-glycoprotein I antibodies. Arthritis Rheum 1999;42:2461–70.
30. Tincani A, Spatola L, Prati E, Allegri F, Ferremi P, Cattaneo R, et al. The anti-β_2-glycoprotein I activity in human anti-phospholipid syndrome sera is due to monoreactive low-affinity autoantibodies directed to epitopes located on native β_2-glycoprotein I and preserved during species' evolution. J Immunol 1996;157:5732–8.
31. Saxena A, Gries A, Schwarzenbacher R, Kostner GM, Laggner P, Prassl R. Crystallization and preliminary x-ray crystallographic studies on apolipoprotein H (β_2-glycoprotein-I) from human plasma. Acta Crystallogr D Biol Crystallogr 1998;54:1450–2.
32. Ito H, Matsushita S, Tokano Y, Nishimura H, Tanaka Y, Fujisao S, et al. Analysis of T cell responses to the β_2-glycoprotein I-derived peptide library in patients with anti-β_2-glycoprotein I antibody-associated autoimmunity. Hum Immunol 2000;61:366–77.
33. Arai T, Yoshida K, Kaburagi J, Inoko H, Ikeda Y, Kawakami Y, et al. Autoreactive CD4+ T-cell clones to β_2-glycoprotein I in patients with antiphospholipid syndrome: preferential recognition of the major phospholipid-binding site. Blood 2001;98:1889–96.

Pkd1 regulates immortalized proliferation of renal tubular epithelial cells through p53 induction and JNK activation

Saori Nishio,[1,2] Masahiko Hatano,[2] Michio Nagata,[3] Shigeo Horie,[4] Takao Koike,[1] Takeshi Tokuhisa,[2] and Toshio Mochizuki[1]

[1]Department of Medicine II, Hokkaido University Graduate School of Medicine, Sapporo, Japan. [2]Department of Developmental Genetics (H2), Graduate School of Medicine, Chiba University, Chiba, Japan. [3]Department of Pathology, Institute of Basic Medical Sciences, University of Tsukuba, Tsukuba, Japan. [4]Department of Urology, Teikyo University School of Medicine, Tokyo, Japan.

Autosomal dominant polycystic kidney disease (ADPKD) is the most common human monogenic genetic disorder and is characterized by progressive bilateral renal cysts and the development of renal insufficiency. The cystogenesis of ADPKD is believed to be a monoclonal proliferation of PKD-deficient ($PKD^{-/-}$) renal tubular epithelial cells. To define the function of *Pkd1*, we generated chimeric mice by aggregation of $Pkd1^{-/-}$ ES cells and $Pkd1^{+/+}$ morulae from ROSA26 mice. As occurs in humans with ADPKD, these mice developed cysts in the kidney, liver, and pancreas. Surprisingly, the cyst epithelia of the kidney were composed of both $Pkd1^{-/-}$ and $Pkd1^{+/+}$ renal tubular epithelial cells in the early stages of cystogenesis. $Pkd1^{-/-}$ cyst epithelial cells changed in shape from cuboidal to flat and replaced $Pkd1^{+/+}$ cyst epithelial cells lost by JNK-mediated apoptosis in intermediate stages. In late-stage cysts, $Pkd1^{-/-}$ cells continued immortalized proliferation with downregulation of p53. These results provide a novel understanding of the cystogenesis of ADPKD patients. Furthermore, immortalized proliferation without induction of p53 was frequently observed in 3T3-type culture of mouse embryonic fibroblasts from $Pkd1^{-/-}$ mice. Thus, *Pkd1* plays a role in preventing immortalized proliferation of renal tubular epithelial cells through the induction of p53 and activation of JNK.

Introduction

Autosomal dominant polycystic kidney disease (ADPKD) is the most common human monogenic genetic disorder and is characterized by progressive bilateral renal enlargement with numerous cysts and fibrosis in the renal parenchyma. It is often accompanied by extra-renal manifestations, such as hypertension, intracranial aneurysms, and hepatic and pancreatic cysts (1). The disease is progressive, and many patients develop renal insufficiency in the fifth and sixth decades of life. Cystogenesis has been studied by microdissection of ADPKD kidneys. The initial event in cyst formation is believed to be the dilatation and "out-pocketing" of tubules. The cysts arise from any segment of one nephron and maintain continuity with the "parental" nephron (2). Fully developed cysts are apparently isolated from the "parental" nephron and expand through the accumulation of cyst fluid (3).

The *PKD1* gene (encoding polycystin-1) (4) and the *PKD2* gene (encoding polycystin-2) (5) have been identified by positional cloning as being the genes responsible for ADPKD. Loss of heterozygosity or second somatic mutations at the *PKD1* or *PKD2* loci have been reported in cystic epithelia from ADPKD patients (6–10). Several lines of mice in which the *Pkd1* or *Pkd2* gene was targeted show similar phenotypes. Although heterozygous knockout mice develop renal and hepatic cysts later in life (after age 16 months) (11), those mice do not fully recapitulate the severity of human ADPKD. Homozygous knockout mice die in utero and develop severely polycystic kidneys (12–16). Interestingly, compound heterozygous $Pkd2^{WS/S}$ mice, which carry a unique *Pkd2* allele that is prone to genomic rearrangement leading to a null allele, develop severely polycystic kidneys during adulthood and thus resemble the ADPKD phenotypes (12). These model animals suggested that a "2-hit" mechanism at either the *PKD1* or *PKD2* gene explains the late onset of the disease as well as some of the variation in clinical symptoms (17, 18).

The molecular mechanisms of the cyst formation of Pkd-deficient ($Pkd^{-/-}$) renal tubular epithelial cells have been studied extensively. Polycystin-1 and polycystin-2 are localized in the primary cilium of renal tubular epithelial cells (19). The relationship between cystogenesis and the disruption of cilia has been reported (20, 21). Although polycystin-2 in node monocilia contributes to the development of left-right asymmetry (22), polycystin-1 and polycystin-2 in the primary cilium transduce the extracellular mechanical stimulus induced by urinary flow into increases in cytosolic Ca^{2+}, which may regulate renal tube size (19, 23).

The cyst epithelial cells of ADPKD kidneys have a high mitotic rate in vitro (24) and in vivo, as detected by immunostaining for proliferating cell nuclear antigen (PCNA) (25), c-Myc, and Ki-67 (26). Their high mitotic rate has also been supported by the following results. First, expression of growth factors such as EGF and their receptors increases in ADPKD cysts (3, 27). Second, cAMP stimulates the in vitro proliferation of ADPKD cyst epithelium and cyst growth (28, 29). Third, overexpression of the *Pkd1* gene in a cell line induced cell cycle arrest at the G0/G1 phase with upregulation of p21 through activation of the JAK-STAT pathway (30). Thus, the proliferation of a $PKD^{-/-}$ cyst epithelial cell might explain the cystogenesis of ADPKD kidneys. However, polycystin-1

Nonstandard abbreviations used: ADPKD, autosomal dominant polycystic kidney disease; DBA, *Dolichos biflorus* agglutinin; LZ, LacZ; MEF, mouse embryonic fibroblast; p-, phosphorylated; PCNA, proliferating cell nuclear antigen.

Conflict of interest: The authors have declared that no conflict of interest exists.

Citation for this article: *J. Clin. Invest.* 115:910–918 (2005). doi:10.1172/JCI200522850.

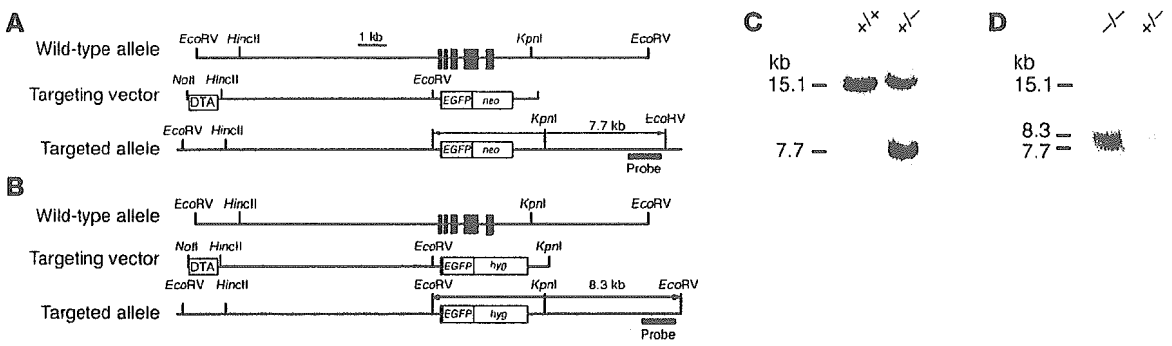

Figure 1

Generation of *Pkd1*$^{-/-}$ ES cells. (**A** and **B**) Genomic organization of 2 targeting vectors. Exons are depicted as filled boxes. The targeting vectors were designed to replace a DNA segment of exons 2–6 by a neomycin-resistance gene cassette (*neo*) (**A**) or a hygromycin-resistance gene cassette (*hyg*) (**B**). *EGFP*, gene encoding enhanced GFP. (**C** and **D**) Southern blots of genomic DNA derived from ES clones. Purified DNA was digested with *Eco*RV and bands were detected by a probe, as described in Methods. Fragments corresponding to wild-type (15.1 kb) and targeted (7.7 kb and 8.3 kb) alleles are shown. +/+, wild-type; –/–, *Pkd1*$^{-/-}$.

and polycystin-2 can be detected in some of the cyst epithelial cells of ADPKD kidneys (31–36). These results suggest a contribution of normal renal tubular epithelial cells to cystogenesis.

The cystogenesis of ADPKD kidneys cannot be fully reproduced in the kidneys of *Pkd1*$^{-/-}$ mice, because these mice die in utero and their renal tubular epithelial cells are not mosaic for *Pkd1*$^{-/-}$ and normal cells, as are ADPKD kidneys. In an attempt to establish an animal model for human ADPKD, we generated chimeric mice by an aggregation method using *Pkd1*$^{-/-}$ ES cells and normal morulae from LacZ^{+} (LZ^{+}) ROSA26 mice (37). We show here that chimeric mice with a low degree of chimerism survived for more than 1 month and had multiple cysts not only in the kidneys but also in the liver and pancreas, suggesting this may be a feasible model for human ADPKD. Surprisingly, both *Pkd1*$^{-/-}$ and wild-type (LZ^{+}) epithelial cells were involved in early cystogenesis in kidneys of the chimeric mice. We discuss here the molecular mechanisms of the cystogenesis of *Pkd1*$^{-/-}$ and *Pkd1*$^{+/+}$ renal tubular epithelial cells.

Results

Cystogenesis of Pkd1$^{-/-}$*/LZ*$^{+}$ *chimeric mice.* We generated mice carrying a mutation in the *Pkd1* gene using standard gene-targeting procedures by replacing exons 2–6 with the neomycin-resistance gene (Figure 1A). Homozygous mutant (*Pkd1*$^{-/-}$) mice died in utero with severely polycystic kidneys and cardiac abnormalities (data not shown), similar to previous descriptions (14, 15). A second targeting vector with the hygromycin-resistance gene (Figure 1B) was transfected into heterozygous (*Pkd1*$^{+/-}$) ES cells to obtain *Pkd1*$^{-/-}$ ES cells. Each gene targeting was confirmed by Southern blot (Figure 1, C and D). Then, we generated chimeric mice composed of mixtures of *Pkd1*$^{-/-}$ and wild-type cells. To monitor cells derived from *Pkd1*$^{-/-}$ ES cells in chimeric mice, we used morulae from LZ^{+} ROSA26 mice. Four independently targeted *Pkd1*$^{-/-}$ ES clones were aggregated with ROSA26 morulae to generate *Pkd1*$^{-/-}$/LZ^{+} chimeric mice.

Several *Pkd1*$^{-/-}$/LZ^{+} mice survived beyond 1 month of age, and their survival closely depended on the degree of chimerism, as estimated by coat color. When the contribution of *Pkd1*$^{-/-}$ ES cells to coat color was more than 30%, the chimeric mice either died in utero or died by P7 with severely polycystic kidneys. *Pkd1*$^{-/-}$/LZ^{+} mice with a lower contribution (less than 10%) of *Pkd1*$^{-/-}$ ES cells to their coat color survived beyond 1 month of age. Renal cysts were detected in all the *Pkd1*$^{-/-}$/LZ^{+} mice examined (n = 90). When we compared chimerism and cyst formation in P7 *Pkd1*$^{-/-}$/LZ^{+} kidneys, the incidence of cysts roughly correlated with the degree of chimerism (Figure 2, A and B). *Pkd1*$^{-/-}$/LZ^{+} kidneys were enlarged due to scattered tubular cysts observed in both the cortex and the outer medulla. These cysts occupied roughly 20–90% of the cut surface of the kidneys, in parallel with the degree of chimerism. A P60 *Pkd1*$^{-/-}$/LZ^{+} mouse had bilateral enlarged kidneys deformed by many cysts and often accompanied by hemorrhage (Figure 2C). Cut surfaces of the kidney showed little renal parenchyma (Figure 2D). This mouse also exhibited hepatic and pancreatic cysts. These pathological findings in *Pkd1*$^{-/-}$/LZ^{+} mice with low degree of chimerism were similar to those of human ADPKD.

To examine initial cyst formation in kidneys of *Pkd1*$^{-/-}$/LZ^{+} and *Pkd1*$^{-/-}$ mice, we microdissected a single nephron from the kidneys of those mice at E17.5. As shown in Figure 2E, multiple "out-pocketing" cysts were observed in all segments of the nephron from *Pkd1*$^{-/-}$/LZ^{+} mice, whereas cysts in the nephrons from *Pkd1*$^{-/-}$ mice were confined mainly to the distal tubule. Surprisingly, the cyst epithelia in chimeric mice were composed of not only *Pkd1*$^{-/-}$ cells but also LZ^{+} wild-type cells, as detected by β-gal staining (Figure 2F). Histochemical examination also showed the presence of LZ^{+} wild-type cells in the cyst epithelia of *Pkd1*$^{-/-}$/LZ^{+} kidneys (Figure 2G).

Dedifferentiation of cyst epithelial cells in Pkd1$^{-/-}$*/LZ*$^{+}$ *mice.* Cystogenesis in kidneys of *Pkd1*$^{-/-}$/LZ^{+} mice with low degree of chimerism was analyzed histologically between P1 and P30. At the early stage (P1), small cysts were numerous and their cyst epithelia were composed of many LZ^{+} cells and some *Pkd1*$^{-/-}$ cells (Figure 3A). At the late stage (P30), individual cysts were enlarged and most of the cyst epithelia were composed of *Pkd1*$^{-/-}$ cells. Similar histological findings were observed in the livers of *Pkd1*$^{-/-}$/LZ^{+} mice (data not shown). Morphological analysis of cyst epithelial cells at the early stage of cystogenesis demonstrated that many of the cyst epithelial *Pkd1*$^{-/-}$ and LZ^{+} cells were cuboidal in shape (Figure 3B). Although the shape of LZ^{+} cyst epithelial cells was still cuboidal at the intermediate stage of cystogenesis, many *Pkd1*$^{-/-}$ cyst epithelial cells changed their shape from cuboidal to flat (Figure 3C), suggesting that flat cyst epithelial cells are dedifferentiated.

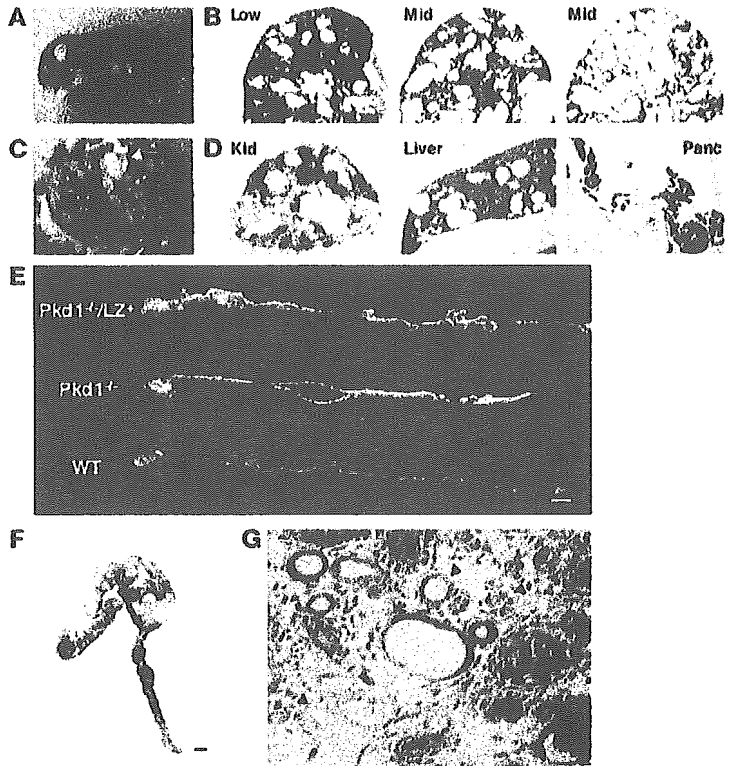

Figure 2

Pkd1$^{-/-}$/LZ^{+} mice as an animal model of human ADPKD. (**A**) Appearance of a P7 *Pkd1*$^{-/-}$/LZ^{+} mouse with an intermediate chimeric rate. The chimeric rate was estimated by coat color. (**B**) Kidneys of P7 *Pkd1*$^{-/-}$/LZ^{+} mice. Low and Mid (intermediate) indicate the chimeric rate as estimated by coat color: Low, less than 10%; Mid, 10% to approximately 30%. (**C**) Kidneys of a P60 *Pkd1*$^{-/-}$/LZ^{+} mouse. Black arrowheads indicate hemorrhagic cysts; white arrowhead indicates pancreatic cysts. (**D**) Cross sections of kidney (Kid), liver, and pancreas (Panc) of a P60 *Pkd1*$^{-/-}$/LZ^{+} mouse. Approximately 90% of the renal parenchyma is occupied by large cysts (PAS staining). Liver and pancreas show numerous cysts (H&E). Original magnification, ×2 (kidney) and ×2.5 (liver and pancreas). (**E**) Single nephrons of *Pkd1*$^{-/-}$/LZ^{+}, *Pkd1*$^{-/-}$, and wild-type mice at E17.5. Multiple "out-pocketing" cysts are present in all segments of the nephron from the *Pkd1*$^{-/-}$/LZ^{+} mouse. Cystic dilation begins at the distal tubule of the nephron of the *Pkd1*$^{-/-}$ mouse. Scale bar: 100 μm. (**F**) Staining of a microdissected tubule with β-gal. A cystic fragment of the *Pkd1*$^{-/-}$/LZ^{+} mouse was composed of *Pkd1*$^{+/+}$ (blue; LZ^{+}) and *Pkd1*$^{-/-}$ (white; LZ^{-}) cells. Scale bar: 100 μm. (**G**) Histochemical analysis of the kidney of a *Pkd1*$^{-/-}$/LZ^{+} mouse at E17.5 with β-gal. The cyst (*) began at tubules involving *Pkd1*$^{-/-}$ (LZ^{-}) and LZ^{+} cells. Some tubules composed of LZ^{-} cells (black arrowheads) showed no cystic dilatation. Counterstaining: Nuclear Fast Red. Original magnification, ×400.

To examine dedifferentiation of flat cyst epithelial cells, we examined expression of polycystin-2 and acetylated tubulin as a marker of primary cilia in the cyst epithelial cells of *Pkd1*$^{-/-}$/LZ^{+} kidneys. All of the cyst epithelial cells expressed polycystin-2 regardless of morphological changes and *Pkd1* expression (Figure 4A), and both LZ^{+} and *Pkd1*$^{-/-}$ (LZ^{-}) cyst epithelial cells manifested cilia (Figure 4B). However, some of the cyst epithelial cells had lost expression of *Dolichos biflorus* agglutinin (DBA) lectins (Figure 4C) and Na-K ATPase (Figure 4D). The loss of expression did not correlate with loss of the *Pkd1* gene in cyst epithelial cells. The mean cell height of cyst epithelial cells with or without Na-K ATPase was lower than that of normal epithelial cells ($P < 0.001$), and the cell height of cyst epithelial cells without Na-K ATPase was slightly lower than that of cyst epithelial cells with Na-K ATPase ($P = 0.029$) (Figure 4E), indicating a tendency of correlation between the dedifferentiation and the flat shape of cyst epithelial cells.

Proliferation and apoptosis of cyst epithelial cells. Immunohistochemistry of cyst epithelial cells in *Pkd1*$^{-/-}$/LZ^{+} kidneys revealed that LZ^{+} cells occasionally showed focal hyperplastic features (Figure 5A) such as micropolyps, as observed in human ADPKD. Some of cuboidal cyst epithelial cells were accompanied by PCNA expression (Figure 5B). We investigated expression of the cell cycle regulators p21 and p53 in *Pkd1*$^{-/-}$/LZ^{+} kidneys by Western blot. Although very low expression of p21 has been reported in the whole body of *Pkd1*$^{-/-}$ embryos at E15.5 (30), the amount of p21 in the kidneys of *Pkd1*$^{-/-}$ embryos at E16.5 and *Pkd1*$^{-/-}$/LZ^{+} mice 1 month of age was slightly less than that in wild-type mice (Figure 5C). Statistical analysis of the amount of p21 in 4 independent experiments indicated a significant difference between wild-type kidneys and *Pkd1*$^{-/-}$ kidneys ($P = 0.016$) but no difference between wild-type kidneys and *Pkd1*$^{-/-}$/LZ^{+} kidneys ($P = 0.107$). Interestingly, the amount of p53 in *Pkd1*$^{-/-}$ ($P = 0.003$) and *Pkd1*$^{-/-}$/LZ^{+} ($P = 0.044$) kidneys was reduced compared with that in wild-type kidneys. Indeed, the amount of p53 decreased in the cuboidal cyst epithelial cells as well as in the flat cyst epithelial cells of *Pkd1*$^{-/-}$/LZ^{+} kidneys (Figure 5D).

To examine the proliferation of cyst epithelial cells in vitro, we cultured microdissected single nephrons with cysts from *Pkd1*$^{-/-}$/LZ^{+} kidneys in collagen gel with 10% FCS. Cells in cystically dilated parts of the nephrons rapidly proliferated in a sheet-like fashion within 18 hours (Figure 5, E–G). Although the great majority were *Pkd1*$^{-/-}$ cells, some LZ^{+} cyst epithelial cells proliferated. This significant proliferation of *Pkd1*$^{-/-}$ and LZ^{+} cyst epithelial cells was sustained by FCS, as a less significant proliferation was observed in collagen gel without FCS (data not shown).

Cyst epithelia at the early stage of cystogenesis were composed of cuboidal *Pkd1*$^{-/-}$ and LZ^{+} cells in *Pkd1*$^{-/-}$/LZ^{+} kidneys, then flat *Pkd1*$^{-/-}$ cells became dominant in cyst epithelia at the intermediate stage. As there were many apoptotic cells present in *Pkd1*$^{-/-}$/LZ^{+} kidneys at the intermediate stage (data not shown), the cuboidal LZ^{+} cells in the cyst epithelia might have been dead due to apoptosis and then filled with flat *Pkd1*$^{-/-}$ cells. Indeed, TUNEL staining of the cyst epithelial cells in *Pkd1*$^{-/-}$/LZ^{+} kidneys revealed scattered TUNEL-positive cells (Figure 6A). Apoptosis in LZ^{+} cyst epithelial cells was 3- to 4-fold larger than that in *Pkd1*$^{-/-}$ cyst epithelial cells (Figure 6B). Electron microscopic analysis of the cyst epithelia showed occasional apoptotic figures in cuboidal cells overlaid by neighboring cells (Figure 6C). In addition, flat cells overlaid several degenerated cells that were detached from the tubular basement membrane (Figure 6D), suggesting rearrangement by flat *Pkd1*$^{-/-}$ cells.

Signaling pathways in relation to proliferation or apoptosis of cyst epithelial cells. Signaling pathways related to cell proliferation were analyzed in the kidneys of *Pkd1*$^{-/-}$ and *Pkd1*$^{-/-}$/LZ^{+} mice. Phosphorylated EGFR (p-EGFR) detected in the cyst epithelial cells of *Pkd1*$^{-/-}$/LZ^{+} kidneys was significantly greater than in those of wild-type kidneys

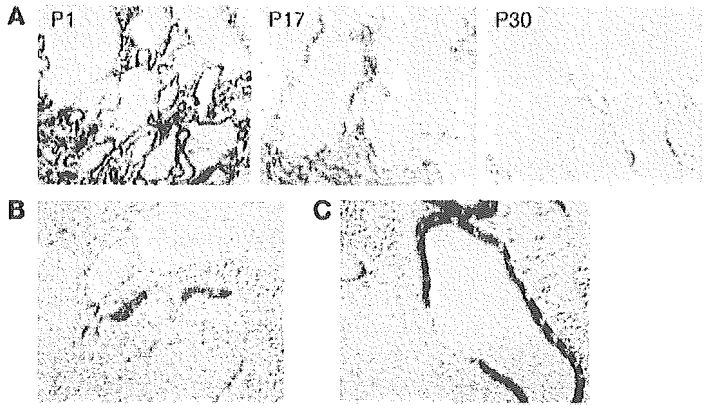

Figure 3
Histochemical analysis of *Pkd1*$^{-/-}$/LZ^{+} kidneys. Kidneys of *Pkd1*$^{-/-}$/LZ^{+} mice were stained with β-gal and counterstained with Nuclear Fast Red. (**A**) Kidneys of *Pkd1*$^{+/-}$/LZ^{+} mice with the low chimeric rate at P1, P17, and P30. At the early stage (P1), cyst epithelia were composed of *Pkd1*$^{-/-}$ (LZ^{-}) and LZ^{+} cells. At the late stage (P30), individual cysts were enlarged and most cyst epithelia were composed of *Pkd1*$^{-/-}$ (LZ^{-}) cells. Original magnification, ×200. (**B**) Kidney of a P3 *Pkd1*$^{-/-}$/LZ^{+} mouse with the intermediate chimeric rate. At the early stage of cystogenesis, both *Pkd1*$^{-/-}$ (LZ^{-}) and LZ^{+} cyst epithelial cells are cuboidal in shape. Original magnification, ×400. (**C**) Kidney of a P8 *Pkd1*$^{-/-}$/LZ^{+} mouse with the low chimeric rate. Cyst epithelia are composed of flat *Pkd1*$^{+/-}$ (LZ^{-}) cells and cuboidal LZ^{+} cells. *Pkd1*$^{-/-}$ (LZ^{-}) cyst epithelial cells changed their shape from cuboidal to flat. Original magnification, ×200.

(data not shown). To elucidate the downstream signaling pathway of growth factors, we analyzed the amount of activated MAP kinases in kidneys using Western blot and immunohistochemistry. Although the amount of p-ERK in *Pkd1*$^{+/-}$ and *Pkd1*$^{+/-}$/LZ^{+} kidneys was not different from that in wild-type kidneys (Figure 7A), expression of p-ERK was significantly more in the cyst epithelial cells of *Pkd1*$^{-/-}$/LZ^{+} kidneys regardless of their shape, cuboidal (Figure 7B) or flat (data not shown).

As for signaling pathways related to apoptosis, the amount of p-JNK was more in *Pkd1*$^{-/-}$/LZ^{+} kidneys ($P = 0.046$) but less in *Pkd1*$^{+/-}$ kidneys ($P = 0.002$) than in wild-type kidneys. Immunohistochemistry revealed that p-JNK expression was increased in the cuboidal cyst epithelial cells rather than in the flat ones of *Pkd1*$^{-/-}$/LZ^{+} kidneys, suggesting that LZ^{+} cyst epithelial cells with p-JNK expression induce apoptosis. In contrast, the amount of p-p38 in *Pkd1*$^{-/-}$/LZ^{+} and *Pkd1*$^{+/-}$ kidneys was similar to that in wild-type kidneys. Furthermore, the amount of p-Akt, an apoptotic inhibitory signal, in both *Pkd1*$^{-/-}$ ($P = 0.008$) and *Pkd1*$^{+/-}$/LZ^{+} ($P = 0.037$) kidneys was more than that in wild-type kidneys. Indeed, p-Akt expression was significantly increased in both cuboidal (data not shown) and flat cyst epithelial cells. The amount of Bcl-X_L in *Pkd1*$^{-/-}$/LZ^{+} kidneys was clearly less than that in wild-type kidneys ($P = 0.032$), whereas that in *Pkd1*$^{+/-}$ kidneys was similar to that in wild-type kidneys. The amount of Bcl-2 and Bax in *Pkd1*$^{-/-}$/LZ^{+} and *Pkd1*$^{+/-}$ kidneys was similar to that in wild-type kidneys ($P = 0.224$ and 0.821, respectively). These findings suggest that LZ^{+} cyst epithelial cells are more apoptotic than are *Pkd1*$^{-/-}$ cyst epithelial cells.

Immortalized growth of Pkd1$^{-/-}$ *mouse embryonic fibroblasts.* Most cyst epithelial cells in *Pkd1*$^{-/-}$/LZ^{+} kidneys at the late stage of cystogenesis were *Pkd1*$^{-/-}$ cells, and these grew very well in collagen gel, suggesting a relationship between loss of *Pkd1* and cell immortalization. Because the 3T3 culture protocol of mouse embryonic fibroblasts (MEFs) is one of the well characterized experimental models of cell immortalization (38) and because normal MEFs express *Pkd1* (data not shown), we cultured *Pkd1*$^{-/-}$ MEFs according to the 3T3 protocol. Wild-type MEFs entered a characteristic cell cycle arrest known as cell senescence after passages 8–9 and immortalized cells (2 of 21 wells) appeared stochastically and eventually overtook the senescent cells (Figure 8A). In contrast, immortalized cells appeared in a large number of wells (21 of 24 wells) in *Pkd1*$^{-/-}$ MEF cultures, thereby suggesting a high incidence of immortalization.

Because the amount of the cell cycle regulator p16 increases in MEFs at the senescence stage (39), we analyzed expression of the cell cycle regulators p16, p21, and p53 in *Pkd1*$^{-/-}$ MEFs using Western blot. The amount of these proteins was similar in *Pkd1*$^{-/-}$ and wild-type MEFs until passage 8, whereas the amount of p16 clearly increased in both *Pkd1*$^{-/-}$ and wild-type MEFs after passage 8 (Figure 8B). However, the amount of p53 in *Pkd1*$^{-/-}$ MEFs at pas-

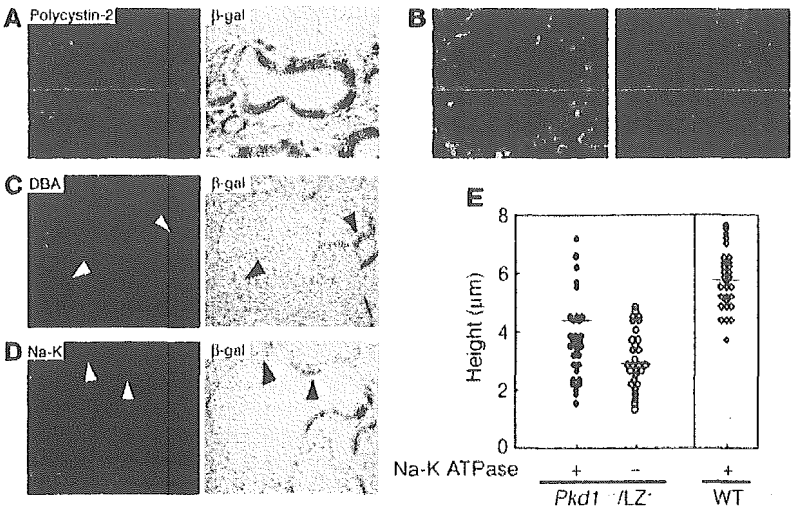

Figure 4
Dedifferentiation of *Pkd1*$^{-/-}$ cyst epithelial cells. (**A–D**) A kidney from a P8 *Pkd1*$^{+/-}$/LZ^{+} mouse was stained with anti–polycystin-2 (red, polycystin-2; blue, DAPI) (**A**), anti–acetylated tubulin (red, acetylated tubulin; green, β-gal; blue, DAPI) (**B**), anti-DBA (**C**) or anti–Na-K ATPase (**D**). (Right panels: **A**, **C**, and **D**) The same section was stained with β-gal and counterstained with Nuclear Fast Red. White and black arrowheads indicate the same epithelial cells. Original magnification, ×400. (**B**) Left and right panels indicate stainings in cuboidal and flat cyst epithelia, respectively. (**E**) Relationship between cell height and Na-K ATPase expression in the cyst epithelial cells shown in **D**. Each symbol indicates a cyst epithelial cell (*Pkd1*$^{-/-}$/LZ^{+}) or normal tubular epithelial cell (WT).

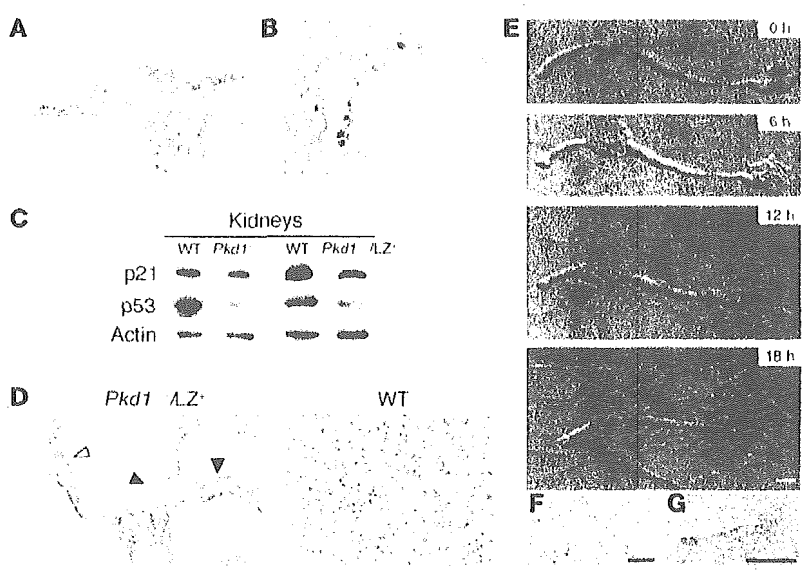

Figure 5
Proliferation of *Pkd1*$^{-/-}$ cyst epithelial cells. (**A**) A kidney from a P17 *Pkd1*$^{-/-}$/LZ^{+} mouse was stained with β-gal and counterstained with Nuclear Fast Red. LZ^{+} epithelial cells occasionally showed focal hyperplastic features such as micropolyps. Original magnification, ×400. (**B**) A kidney froma P12 *Pkd1*$^{-/-}$/LZ^{+} mouse was stained with an anti-PCNA. Some cuboidal LZ^{+} cyst epithelial cells were accompanied by PCNA expression. Original magnification, ×400. (**C**) Expression of p21 and p53 in the kidneys of *Pkd1*$^{-/-}$ mice at E16.5 and *Pkd1*$^{-/-}$/LZ^{+} mice 1 month of age. The amount of p21 and p53 in kidneys was examined using Western blot. Actin was used as a loading control for protein. Data presented are 1 representative of 4 independent experiments. (**D**) Kidneys of P12 *Pkd1*$^{-/-}$/LZ^{+} and P12 wild-type mice were stained with anti-p53. Expression of p53 was detected in the flat epithelial cells (white arrowhead) but was significantly decreased in the cuboidal cyst epithelial cells (black arrowheads) of the *Pkd1*$^{-/-}$/LZ^{+} mouse. Original magnification, ×400. (**E–G**) The proliferation of cyst epithelial cells in vitro. A single nephron isolated by microdissection from the kidney of a *Pkd1*$^{-/-}$/LZ^{+} mouse at E17.5 was cultured in collagen gel for 18 hours. (**F** and **G**) Higher magnifications of the boxed area above. Both LZ^{+} and *Pkd1*$^{-/-}$ (LZ^{-}) cells proliferated. Scale bars: 100 μm.

sage 30 ($P = 0.001$) but not that in wild-type MEFs at passage 13 ($P = 0.636$) was clearly less than that in *Pkd1*$^{-/-}$ and wild-type MEFs at passage 1. The amount of activated MAP kinases in MEFs was examined further. The amount of p-ERK in *Pkd1*$^{-/-}$ MEFs at passage 30 was slightly more than that in wild-type MEFs at passage 13. Although the amount of p-JNK ($P = 0.032$) and p-p38 ($P = 0.038$) increased in wild-type MEFs from passage 8 to passage 13, it was stable in *Pkd1*$^{-/-}$ MEFs until passage 30. The amount of p-Akt in *Pkd1*$^{-/-}$ MEFs was also stable until passage 30. Furthermore, the amount of Bcl-2 family proteins was similar in *Pkd1*$^{-/-}$ and wild-type MEFs at passages 30 and 13, respectively (data not shown).

Discussion

In the present study, we developed *Pkd1*$^{-/-}$/LZ^{+} chimeric mice. The pathological findings in *Pkd1*$^{-/-}$/LZ^{+} kidneys were similar to those in human ADPKD kidneys. Therefore, *Pkd1*$^{-/-}$/LZ^{+} mice, like *Pkd2*$^{WS25/-}$ mice (12), are a feasible model for human ADPKD. As intragenic recombination events in *Pkd2*$^{WS25/-}$ mice occurred gradually and postnatally, as in human ADPKD, whereas *Pkd1*$^{-/-}$/LZ^{+} mice have *Pkd1*$^{-/-}$ cells by inheritance, cyst formation in *Pkd1*$^{-/-}$/LZ^{+} kidneys progressed more rapidly than that in *Pkd2*$^{WS25/-}$ and human ADPKD kidneys. However, with *Pkd1*$^{-/-}$/LZ^{+} mice, we have the advantage of distinguishing *Pkd1*$^{-/-}$ cells from normal (LZ^{+}) cells and of monitoring the contribution of *Pkd1*$^{-/-}$ cells in cystogenesis. Analyses of the cyst epithelial cells in *Pkd1*$^{-/-}$/LZ^{+} kidneys can help us to understand the in vivo effect of polycystin-1 on cystogenesis.

Proliferation of normal tubular epithelial cells in early cystogenesis. Cystogenesis in human ADPKD has been proposed as being a monoclonal proliferation of PKD1- or PKD2-deficient epithelial cells (6–10). However, we found that the cystic epithelium at the early stage of cystogenesis was composed of both *Pkd1*$^{-/-}$ and LZ^{+} wild-type cells. This finding is supported by results showing that expression of polycystin-1 and polycystin-2 was detected in most cultured cells derived from ADPKD kidneys (40). We stress that the strong expression of polycystin-1 and polycystin-2 on cystic epithelia in ADPKD kidneys (31–36) may reflect involvement of normal cyst epithelial cells in the cystogenesis of human ADPKD.

The initial cystogenesis in the kidney with *Pkd1*$^{-/-}$ tubular epithelial cells requires stimulation, as some of the tubules with *Pkd1*$^{-/-}$ epithelial cells occasionally had no cystic dilatation and metanephric culture of organs harvested from *Pkd1*$^{-/-}$ mice at E13.5 failed to show cyst development (data not shown). It has been suggested that urinary flow promotes nephron development, in particular, tubular elongation with cell differentiation (41). During nephron development, it is hypothesized that the renal tubular diameter is maintained at the proper size (23) and that the primary cilium affects the maintenance of the tubular diameter by its mechanosensor function (19, 20). Cilia structure and polycystin-2 expression were manifested in the cyst epithelial cells of *Pkd1*$^{-/-}$/LZ^{+} kidneys. Thus, we surmise that polycystin-1 in the primary cilium is required for further inhibition of the proliferation of tubular epithelial cells to maintain their proper size. A *Pkd1*$^{-/-}$ epithelial cell, which is missing negative regulatory signals from polycystin-1, continuously proliferates, and this proliferation induces a "compensatory" proliferation of the surrounding normal epithelial cells in an attempt to re-establish appropriate tubular diameter and structure. This proliferation of tubular epithelial cells accounts for early cyst formation in human ADPKD.

Proliferation of Pkd1$^{-/-}$ *cyst epithelial cells.* EGFR (14, 27), cAMP (28, 29), Wnt/β-catenin (42), and p21 (30) have all been linked to the proliferation of cyst epithelial cells. However, the relationship between activation of these molecules and PKD deficiency is not clear, as those studies assumed that only *PKD*$^{-/-}$ cells proliferated in human ADPKD. Although downregulation of p21 expression in whole embryos of *Pkd1*$^{-/-}$ mice has been suggested to be involved in the proliferation of cyst epithelial cells (30) and we reproduced this downregulation in *Pkd1*$^{-/-}$ kidneys, p21 expression in *Pkd1*$^{-/-}$/LZ^{+} kidneys revealed only a slight decrease. The expression of p53 was significantly decreased in the kidneys of *Pkd1*$^{-/-}$ and *Pkd1*$^{-/-}$/LZ^{+} mice. These results support the findings that p53 expression is decreased in human embryonic kidney 293 cells with loss of polycystin-1 activity (43) and is also slightly decreased in human

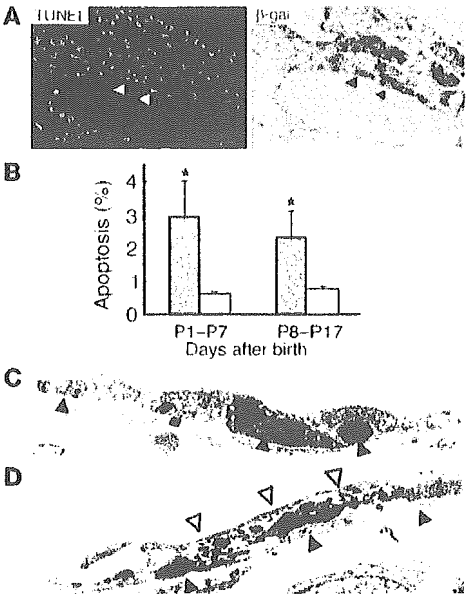

Figure 6
Apoptosis of cyst epithelial cells. (**A**) Apoptosis of cyst epithelial cells in the kidney of a P8 *Pkd1*$^{-/-}$/LZ^{+} mouse was detected by the TUNEL assay. The same section was stained with β-gal and counterstained with Nuclear Fast Red. Arrowheads indicate TUNEL-positive cells. Original magnifications, ×400. (**B**) Summary of results shown in **A**. Each graph represents the percentage of TUNEL-positive cells in LZ^{+} (black bars) and in LZ^{-} (*Pkd1*$^{-/-}$) cyst epithelial cells (white bars), respectively. The mean and SD are from 9 independent mice. $^{*}P < 0.05$. (**C** and **D**) Electron microscopic analysis of the cyst epithelium of a *Pkd1*$^{-/-}$/LZ^{+} kidney. (**C**) Occasional apoptotic cells (black arrowheads) are overlaid by neighboring cells. (**D**) Flat cells (white arrowheads) overlay several degenerated cells that are detached from the tubular basement membrane (black arrowheads). Original magnification, ×1,500.

ADPKD kidneys compared with normal kidneys (26). p53 inhibits cell cycle by induction of p21 (44), and polycystin-1 inhibits Cdk2 activity by upregulation of p21 through the activation of JAK2 (30). Thus, the decrease in p53 in addition to the lack of activation of the JAK-STAT pathway in Pkd1 deficiency may compound the decrease in p21 expression. Because expression of p53, among the cell cycle regulators examined, was affected most strongly in both *Pkd1*$^{-/-}$ cyst epithelial cells and immortalized *Pkd1*$^{-/-}$ MEFs, polycystin-1 may regulate the growth of renal tubular epithelial cells through induction of p53.

Pkd1$^{-/-}$ cyst epithelial cells were not transplantable in nude mice (data not shown). Isolated early cysts from *Pkd1*$^{-/-}$/LZ^{+} kidneys exhibited significant proliferation in vitro with 10% FCS, whereas the proliferation was stunted without FCS (data not shown), suggesting that proliferation of *Pkd1*$^{-/-}$ cyst epithelial cells is not autonomous, as in neoplasms, but instead is growth factor dependent. Among many growth factors and their receptors related with cystogenesis, strong EGFR expression was observed on cystic epithelia of *Pkd1*$^{-/-}$ kidneys (14). Interestingly, EGFR expression increased on both cuboidal and flat cyst epithelial cells in *Pkd1*$^{-/-}$/LZ^{+} kidneys (data not shown). This was supported by the finding of scattered activation of the ERK pathway in both cuboidal and flat cyst epithelial cells in *Pkd1*$^{-/-}$/LZ^{+} kidneys.

Dedifferentiation of Pkd1$^{-/-}$ *cyst epithelial cells.* The cyst epithelia in human ADPKD are composed of cuboidal cells such as normal renal epithelial cells and flat cells (24). A similar phenomenon was noted in *Pkd2*^{WS25} kidneys. These 2 morphologically different cells constitute the cyst epithelium at the early and intermediate stages of cystogenesis (45). We also detected 2 kinds of cyst epithelial cells in *Pkd1*$^{-/-}$/LZ^{+} kidneys. Both *Pkd1*$^{-/-}$ and LZ^{+} cyst epithelial cells were cuboidal in shape at the early stage of cystogenesis, and some *Pkd1*$^{-/-}$ cyst epithelial cells changed their shape to flat at the intermediate stage. As LZ^{+} cyst epithelial cells are nearly cuboidal, Pkd1 deficiency is related to the morphological change.

Most flat cyst epithelial cells are negative for nephron segment markers and Na-K ATPase (45), suggesting that the morphological transition of *Pkd1*$^{-/-}$ cyst epithelial cells is accompanied by loss of functional phenotype. However, expression of renal tubular markers within single cysts in *Pkd1*$^{-/-}$/LZ^{+} kidneys was discontinuous. Loss of expression was also detected in the cuboidal cyst epithelial cells at the early stage of cystogenesis. Although there is a tendency for correlation between loss of Na-K ATPase expression and flat shape of cyst epithelial cells, the morphological change of cyst epithelial cells is not completely correlated with the loss of tubular markers.

The cell adhesion molecules E-cadherin and β-catenin are bound to polycystin-1 and polycystin-2 (42), and E-cadherin expression decreases in *Pkd1*$^{-/-}$ kidneys (14). Thus, Pkd1 deficiency may change the polarity of cyst epithelial cells by affecting cell adhesion or

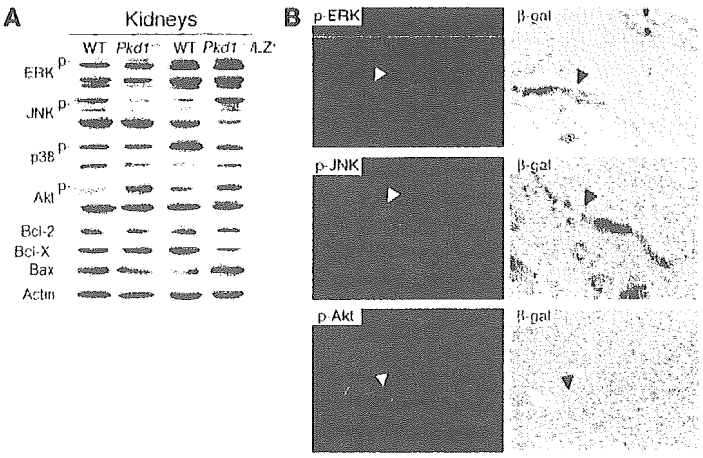

Figure 7
Signaling pathways related to proliferation or apoptosis in cyst epithelial cells. (**A**) Expression of signal transducers in the kidneys of *Pkd1*$^{-/-}$ mice at E16.5 and *Pkd1*$^{-/-}$/LZ^{+} mice 1 month of age was analyzed using Western blot. Actin was used as a loading control for protein. Data presented are 1 representative of 4 independent experiments. (**B**) A kidney from a P8 *Pkd1*$^{-/-}$/LZ^{+} mouse was stained with anti–p-ERK, anti–p-JNK, or anti–p-Akt. The same section was stained with β-gal and counterstained with Nuclear Fast Red. Black and white arrowheads indicate the same epithelial cells. Original magnification, ×400.

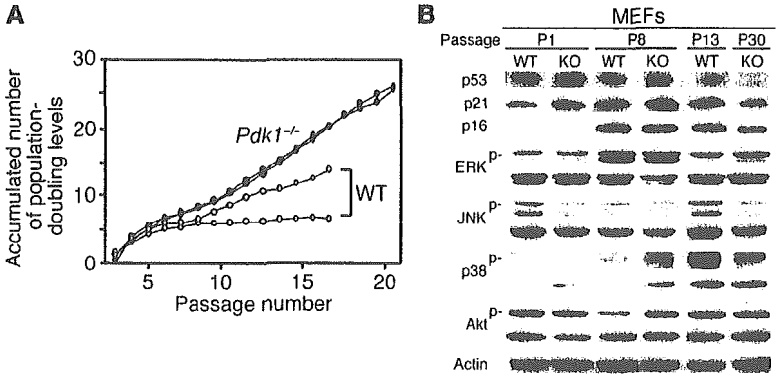

Figure 8
Outgrowing *Pkd1*$^{-/-}$ MEFs. (**A**) The 3T3-type culture of MEFs from *Pkd1*$^{-/-}$ and wild-type mice. (**B**) Signaling pathways related to proliferation or apoptosis in *Pkd1*$^{-/-}$ MEFs. Expression of signal transducers and cell cycle regulators was analyzed using Western blot. Actin was used as a loading control for protein. Data presented are 1 representative of 4 independent experiments.

cytoskeletal organization. However, the localization and intensity of both E-cadherin and β-catenin in some cyst epithelial cells were similar to those in normal renal tubular cells at the intermediate stage of cystogenesis (data not shown). These results indicate that the morphological change in cyst epithelial cells is not due to loss of tubular markers or to repression of cell adhesion molecules. As *Pkd1*$^{-/-}$ cyst epithelial cells cultured in collagen gel sometimes made tubules in the gel (data not shown), outgrowing *Pkd1*$^{-/-}$ cyst epithelial cells retain some functions of renal tubular epithelial cells. Further studies will be done to elucidate the cause of the morphological change and the dedifferentiation (loss of tubular markers) of cyst epithelial cells initiated by deficiency in the *Pkd1* gene.

Apoptosis on normal (LZ^{+}*) cyst epithelial cells.* Apoptosis has been frequently observed in non-dilated and cystic tubuli and glomeruli in ADPKD kidneys, whereas it is extremely rare in normal kidneys (46). In addition, the increased rate of growth in cyst epithelial cells is accompanied by an increased rate of apoptosis in human ADPKD (26). Of note, our study showed that apoptotic cells were present mainly in cuboidal epithelial cells in *Pkd1*$^{-/-}$/LZ^{+} kidneys. Electron microscopy revealed characteristic apoptotic features among cuboidal cyst epithelium, which was covered by flat cells. Apoptotic cells were lost from cyst epithelium and neighboring flat cells lined tubular lumina. These findings suggest net replacement of cuboidal LZ^{+} epithelial cells by flat *Pkd1*$^{-/-}$ epithelial cells.

Expression of p-JNK increased in *Pkd1*$^{-/-}$/LZ^{+} kidneys but not in *Pkd1*$^{-/-}$ kidneys. In contrast, Bcl-X_L expression was decreased in *Pkd1*$^{-/-}$/LZ^{+} kidneys but not in *Pkd1*$^{-/-}$ kidneys. Although p-Akt expression was significantly increased in both cuboidal and flat cyst epithelial cells, cuboidal cyst epithelial cells are more apoptotic than are flat cyst epithelial cells. The 3T3 cell cultures using *Pkd1*$^{-/-}$ MEFs also demonstrated that expression of p-JNK and p-p38 was increased in wild-type MEFs at the cell senescence stage (after passage 13). However, this expression did not increase in immortalized *Pkd1*$^{-/-}$ MEFs until passage 30. As polycystin-1 triggers activation of JNK but not that of p38 (47), flat *Pkd1*$^{-/-}$ epithelial cells and *Pkd1*$^{-/-}$ MEFs in the 3T3 culture escape apoptosis mediated by activation of JNK. These immortalized flat *Pkd1*$^{-/-}$ epithelial cells slowly spread to form large cysts.

A model of cystogenesis. We developed chimeric mice by aggregation of *Pkd1*$^{-/-}$ ES cells and *Pkd1*$^{+/+}$ morulae of LZ^{+} ROSA26 mice. These mice are a unique mouse model for human ADPKD. In *Pkd1*$^{-/-}$/LZ^{+} kidneys, sporadic *Pkd1*$^{-/-}$ epithelial cells deteriorated the entire tubular integrity by the proliferation of both *Pkd1*$^{-/-}$ and normal (LZ^{+}) epithelial cells at the early stage of cystogenesis (Figure 9). When tubular epithelial cells, including *Pkd1*$^{-/-}$ epithelial cells, receive stimulation, both *Pkd1*$^{-/-}$ and normal tubular epithelial cells proliferate to expand the tubular size. The *Pkd1*$^{-/-}$ tubular epithelial cells lack negative signals for proliferation by polycystin-1 and continue to proliferate. Although surrounding normal tubular epithelial cells also proliferate to retain both the round shape and diameter of the tubule, normal epithelial cells are gradually lost by JNK-mediated apoptosis at the intermediate stage. Some *Pkd1*$^{-/-}$ tubular epithelial cells change shape from cuboidal to flat (dedifferentiation), and the flat *Pkd1*$^{-/-}$ epithelial cells grow in an immortalized fashion to form large cysts in the kidney at the late stage of cystogenesis. As p53 expression and JNK activation were very low in flat *Pkd1*$^{-/-}$ cyst epithelial cells, polycystin-1 plays a role in the prevention of immortalized proliferation of renal tubular epithelial cells via p53 induction and JNK activation.

Methods

Generation of Pkd1$^{-/-}$ *mice.* Murine *Pkd1* genomic clones were obtained by screening a 129/Sv mouse genomic library (14). R1 ES cells were transfected with linearized *Pkd1* neomycin-targeting vectors by electroporation and were subjected to positive and negative selection for 14 days using G418 and diphtheria toxin. Approximately 134 clones were examined using Southern blot, and homologous recombination was detected in 18 clones. One independent targeted ES clone was used to generate chimeric mice using the aggregation method (48). DNA from tail tissue of agouti pups

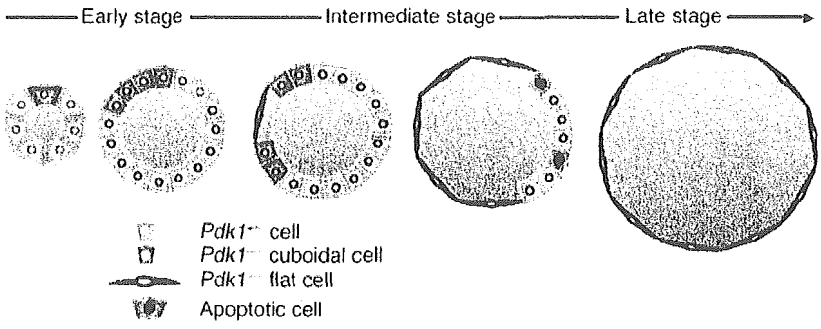

Figure 9
A model schema of the cystogenesis in ADPKD. The germline mutation of 1 allele of the *Pkd1* gene is present in all tubular epithelial cells.

obtained by mating chimeric mice with C57BL/6 mice (Japan SLC) was analyzed using Southern blot. Homozygous mutant pups were generated by intercrossing of heterozygous mutant mice. All procedures conformed to the Chiba University Resolution on Use of Animals in Research and were approved by the Institutional Animal Care and Use Committee of the Graduate School of Medicine, Chiba University (Chiba, Japan).

Generation of Pkd1 ES cells and Pkd1 LZ chimeric mice. One of the *Pkd1*-targeted ES clones was transfected by electroporation with linearized *Pkd1* hygromycin targeting vectors to generate *Pkd1* ES cells. Approximately 17 ES clones were examined by Southern blot, and 4 independent *Pkd1* ES clones were obtained. Those *Pkd1* ES cells were aggregated with morulae of ROSA26 mice with the exogenous *LacZ* gene (a gift from H. Koseki, RIKEN Research Center for Allergy and Immunology, Yokohama, Japan) to generate *Pkd1* /LZ chimeric mice.

Southern blot. Genotyping was done by digestion of genomic DNA (10 μg) with *Eco*RV, Southern transfer, and hybridization with a 1.3-kb DNA probe that was external to the targeting vector. The probe was labeled with digoxigenin (Roche Diagnostics) using PCR. The probe detected the wild-type allele as a 15.1-kb fragment and the mutant alleles as 7.7-kb and 8.3-kb fragments.

Histology and immunohistochemistry. Tissues were fixed in 10% phosphate-buffered formalin and were embedded in paraffin. Sections (3 μm thick) were stained with H&E according to standard protocols. For immunohistochemistry, after deparaffinization through a graded xylene and ethanol series, sections were washed in PBS (pH 7.4) and were treated for 15 minutes with 0.3% hydrogen peroxide in methanol. After blocking, sections were stained with the following antibodies: anti-p53, anti-p-EGFR (Santa Cruz Biotechnology Inc.), and anti-PCNA (Sigma-Aldrich). For immunofluorescence, frozen section were stained with YCC2 (anti-polycystin-2; a kind gift from Y. Cai, Yale University, New Haven, Connecticut, USA), anti-β-gal (Chemicon International Inc.), anti-Na-K ATPase (Upstate), anti-acetylated tubulin, anti-DBA, anti-lectin *Lotus tetragonolobus* (Sigma-Aldrich), anti-p-ERK, anti-p-Akt, or anti-p-JNK (Cell signaling Technology Inc.). Photomicrographs were obtained using a microscope (Carl Zeiss International).

β-gal staining of kidneys. Kidneys were fixed for 30 minutes at 4°C in 2.7% formaldehyde, 0.02% NP-40, and 0.2% glutaraldehyde in PBS (pH 7.4) and were washed. Processing was carried out through a graded series of sucrose concentrations from 15% to 30% in PBS at 4°C for 5–12 hours for each step. Kidneys were then embedded in OCT (Tissue-Tek) and were frozen in 2-methyl-butane submerged in liquid nitrogen. Sections (3 μm thick) were then prepared, mounted on slides, and washed in PBS for 5 minutes, and were subsequently stained at 37°C overnight in X-gal solution (1 mg/ml X-gal in DMSO, 2 mM $MgCl_2$, 20 mM potassium ferricyanide, 20 mM potassium ferrocyanide, and 0.02 % NP-40 in PBS). Sections were counterstained with Nuclear Fast Red (Trevigen Inc.).

Microdissection of nephron segments. Nephrons were isolated from the kidneys of wild-type, *Pkd1* , and *Pkd1* /LZ mice at E17.5. Microdissection of tubules was done in PBS under a stereomicroscope (2).

Western blot. Kidneys were sonicated in Tris lysis buffer (20 mM Tris-HCl, 150 mM NaCl, 100 mM NaF, 1 mM EDTA, 1 mM sodium orthovanadate, 1 mM phenylmethylsulfonyl fluoride, 1.5 nM aprotinin, and 10 nM leupeptin). Proteins were separated by SDS-PAGE and were transferred to polyvinylidene difluoride membranes (Millipore). Membranes were blocked with nonfat dry milk (Yukijirushi) and were incubated with the following antibodies: anti-p53, anti-p21, anti-ERK, anti-Bcl-X_L, anti-Bax, anti-p16, anti-actin (Santa Cruz Biotechnology Inc.), anti-Akt, anti-p-Akt, anti-p-ERK, anti-p38, anti-p-p38 (Cell Signaling Technology Inc.), anti-JNK, anti-p-JNK (BD Biosciences Pharmingen), or anti-Bcl-2 (R&D Systems). The filters were washed with TBS/0.1% Triton-X, and immunoreactive bands were visualized by enhanced chemiluminescence.

In vitro culture of microdissected tubules. Microdissection of tubules was done in L-15 medium (Sigma-Aldrich) followed by culture at 37°C in 5% CO_2 in collagen gel (Neutral Solution, DMEM Culture Medium; Koken) in DMEM supplemented with 10% FCS (Sigma-Aldrich).

TUNEL assay. Animals were perfused with a solution of 4% paraformaldehyde in 0.1 M phosphate buffer (pH 7.4). Organs were dissected and were post-fixed overnight with 4% paraformaldehyde. The tissues were equilibrated with 20% sucrose and were cut into sections 3 μm in thickness on a cryostat. The TUNEL assay was carried as described with slight modification (49). The tailing reaction was carried out for 1 hour at 37°C in TdT buffer in the presence of dUTP-biotin (The Mebstain Apoptosis kit, Medical & Biological Laboratories). Signals were visualized using Avidin-Rohdamine (Vector Laboratories). Sections were counterstained with DAPI (Molecular Probes).

Electron microscopy. Specimens were fixed in formalin followed by 2% glutaraldehyde, were post-fixed with 1% osmium tetroxide, and were embedded in epoxy resin mixture. Ultrathin sections were mounted on grids, stained with uranyl acetate–lead citrate, and observed under a transmission electron microscope (Hitachi).

Cell culture. MEFs were established from *Pkd1* embryos (E13.5). Heads and livers were removed from embryos, and the remaining embryonic tissues were trypsinized at 37°C for 30 minutes. The disrupted tissues were plated in DMEM supplemented with 10% FCS (Sigma-Aldrich) and were cultured at 37°C in 5% CO_2. The 3T3-type serial MEF cultivation was done as described (38). Briefly, 3×10^5 cells were plated on a 6-cm well; 3 days later, the total number of cells was counted, and 3×10^5 cells were plated on a separate well. The cumulative increase in cell number was calculated according to the formula $\mathrm{Log}(N_t / N_i)/\mathrm{Log}2$, where N_i is the initial number of cells plated and N_t is the final number of cells counted after 3 days.

Statistical analysis. Data presented represents the mean ± SD of more than 3 independent experiments. Statistical analysis was performed using an unpaired Student's *t* test. *P* values of less than 0.05 were considered to be significant.

Acknowledgments

We are grateful to H. Koseki and S. Somlo for discussions and to Y. Cai for providing YCC2 (anti-polycystin-2). We also thank L. Fujimura, H. Satake, K. Hanaoka, J. Usui, S. Horita, and H. Hazawa for skillful technical assistance; N. Kakinuma for secretarial services; and M. Ohara for language assistance. This work was supported in part by Grants-in-Aid from the Ministry of Education, Science, Technology, Sports and Culture of Japan, a grant from the Inamori Foundation (to T. Mochizuki), and a grant from Sankyo Foundation of Life Science (to T. Mochizuki).

Received for publication July 28, 2004, and accepted in revised form January 11, 2005.

Address correspondence to: Toshio Mochizuki, Department of Medicine II, Hokkaido University Graduate School of Medicine, Kita 15, Nishi 7, Kita-ku, Sapporo 060-8638, Japan. Phone: 81-11-716-1161; Fax: 81-11-706-7710; E-mail: mtoshi@med.hokudai.ac.jp.

1. Gabow, P.A. 1993. Autosomal dominant polycystic kidney disease. *N. Engl. J. Med.* **329**:332–342.
2. Baert, L. 1978. Hereditary polycystic kidney disease (adult form): a microdissection study of two cases at an early stage of the disease. *Kidney Int.* **13**:519–525.
3. Wilson, P.D. 2004. Polycystic kidney disease. *N. Engl. J. Med.* **350**:151–164.
4. The European Polycystic Kidney Disease Consortium. 1994. The polycystic kidney disease 1 gene encodes a 14 kb transcript and lies within a duplicated region on chromosome 16. The

European Polycystic Kidney Disease Consortium. *Cell* **77**:881–894.
5. Mochizuki, T., et al. 1996. PKD2, a gene for polycystic kidney disease that encodes an integral membrane protein. *Science.* **272**:1339–1342.
6. Watnick, T.J., et al. 1998. Somatic mutation in individual liver cysts supports a two-hit model of cystogenesis in autosomal dominant polycystic kidney disease. *Mol. Cell.* **2**:247–251.
7. Qian, F., Watnick, T.J., Onuchic, L.F., and Germino, G.G. 1996. The molecular basis of focal cyst formation in human autosomal dominant polycystic kidney disease type I. *Cell.* **87**:979–987.
8. Pei, Y., et al. 1999. Somatic PKD2 mutations in individual kidney and liver cysts support a "two-hit" model of cystogenesis in type 2 autosomal dominant polycystic kidney disease. *J. Am. Soc. Nephrol.* **10**:1524–1529.
9. Brasier, J.L., and Henske, E.P. 1997. Loss of the polycystic kidney disease (PKD1) region of chromosome 16p13 in renal cyst cells supports a loss-of-function model for cyst pathogenesis. *J. Clin. Invest.* **99**:194–199.
10. Torra, R., et al. 1999. A loss-of-function model for cystogenesis in human autosomal dominant polycystic kidney disease type 2. *Am. J. Hum. Genet.* **65**:345–352.
11. Lu, W., et al. 1999. Late onset of renal and hepatic cysts in Pkd1-targeted heterozygotes. *Nat. Genet.* **21**:160–161.
12. Wu, G., et al. 1998. Somatic inactivation of Pkd2 results in polycystic kidney disease. *Cell.* **93**:177–188.
13. Lu, W., et al. 1997. Perinatal lethality with kidney and pancreas defects in mice with a targetted Pkd1 mutation. *Nat. Genet.* **17**:179–181.
14. Muto, S., et al. 2002. Pioglitazone improves the phenotype and molecular defects of a targeted Pkd1 mutant. *Hum. Mol. Genet.* **11**:1731–1742.
15. Boulter, C., et al. 2001. Cardiovascular, skeletal, and renal defects in mice with a targeted disruption of the Pkd1 gene. *Proc. Natl. Acad. Sci. U. S. A.* **98**:12174–12179.
16. Lu, W., et al. 2001. Comparison of Pkd1-targeted mutants reveals that loss of polycystin-1 causes cystogenesis and bone defects. *Hum. Mol. Genet.* **10**:2385–2396.
17. Sutters, M., and Germino, G.G. 2003. Autosomal dominant polycystic kidney disease: molecular genetics and pathophysiology. *J. Lab. Clin. Med.* **141**:91–101.
18. Igarashi, P., and Somlo, S. 2002. Genetics and pathogenesis of polycystic kidney disease. *J. Am. Soc. Nephrol.* **13**:2384–2398.
19. Nauli, S.M., et al. 2003. Polycystins 1 and 2 mediate mechanosensation in the primary cilium of kidney cells. *Nat. Genet.* **33**:129–137.
20. Yoder, B.K., Hou, X., and Guay-Woodford, L.M. 2002. The polycystic kidney disease proteins, polycystin-1, polycystin-2, polaris, and cystin, are co-localized in renal cilia. *J. Am. Soc. Nephrol.* **13**:2508–2516.
21. Lin, F., et al. 2003. Kidney-specific inactivation of the KIF3A subunit of kinesin-II inhibits renal ciliogenesis and produces polycystic kidney disease. *Proc. Natl. Acad. Sci. U. S. A.* **100**:5286–5291.
22. McGrath, J., Somlo, S., Makova, S., Tian, X., and Brueckner, M. 2003. Two populations of node monocilia initiate left-right asymmetry in the mouse. *Cell.* **114**:61–73.
23. Lubarsky, B., and Krasnow, M.A. 2003. Tube morphogenesis: making and shaping biological tubes. *Cell.* **112**:19–28.
24. Grantham, J.J., Geiser, J.L., and Evan, A.P. 1987. Cyst formation and growth in autosomal dominant polycystic kidney disease. *Kidney Int.* **31**:1145–1152.
25. Nadasdy, T., et al. 1995. Proliferative activity of cyst epithelium in human renal cystic diseases. *J. Am. Soc. Nephrol.* **5**:1462–1468.
26. Lanoix, J., D'Agati, V., Szabolcs, M., and Trudel, M. 1996. Dysregulation of cellular proliferation and apoptosis mediates human autosomal dominant polycystic kidney disease (ADPKD). *Oncogene.* **13**:1153–1160.
27. Wilson, P.D., Du, J., and Norman, J.T. 1993. Autocrine, endocrine and paracrine regulation of growth abnormalities in autosomal dominant polycystic kidney disease. *Eur. J. Cell Biol.* **61**:131–138.
28. Yamaguchi, T., et al. 2003. Cyclic AMP activates B-Raf and ERK in cyst epithelial cells from autosomal-dominant polycystic kidneys. *Kidney Int.* **63**:1983–1994.
29. Hanaoka, K., and Guggino, W.B. 2000. cAMP regulates cell proliferation and cyst formation in autosomal polycystic kidney disease cells. *J. Am. Soc. Nephrol.* **11**:1179–1187.
30. Bhunia, A.K., et al. 2002. PKD1 induces p21(waf1) and regulation of the cell cycle via direct activation of the JAK-STAT signaling pathway in a process requiring PKD2. *Cell.* **109**:157–168.
31. Ong, A.C., et al. 1999. Polycystin-1 expression in PKD1, early-onset PKD1, and TSC2/PKD1 cystic tissue. *Kidney Int.* **56**:1324–1333.
32. Ward, C.J., et al. 1996. Polycystin, the polycystic kidney disease 1 protein, is expressed by epithelial cells in fetal, adult, and polycystic kidney. *Proc. Natl. Acad. Sci. U. S. A.* **93**:1524–1528.
33. Geng, L., et al. 1996. Identification and localization of polycystin, the PKD1 gene product. *J. Clin. Invest.* **98**:2674–2682.
34. Griffin, M.D., Torres, V.E., Grande, J.P., and Kumar, R. 1996. Immunolocalization of polycystin in human tissues and cultured cells. *Proc. Assn. Am. Physicians.* **108**:185–197.
35. Weston, B.S., et al. 1997. Polycystin expression during embryonic development of human kidney in adult tissues and ADPKD tissue. *Histochem. J.* **29**:847–856.
36. Nauta, J., Goedbloed, M.A., van den Ouweland, A.M., Nellist, M., and Hoogeveen, A.T. 2000. Immunological detection of polycystin-1 in human kidney. *Histochem. Cell Biol.* **113**:303–311.
37. Zambrowicz, B.P., et al. 1997. Disruption of overlapping transcripts in the ROSA beta geo 26 gene trap strain leads to widespread expression of beta-galactosidase in mouse embryos and hematopoietic cells. *Proc. Natl. Acad. Sci. U. S. A.* **94**:3789–3794.
38. Todaro, G.J., and Green, H. 1963. Quantitative studies of the growth of mouse embryo cells in culture and their development into established lines. *J. Cell Biol.* **17**:299–313.
39. Kamijo, T., et al. 1997. Tumor suppression at the mouse INK4a locus mediated by the alternative reading frame product p19ARF. *Cell.* **91**:649–659.
40. Loghman-Adham, M., Nauli, S.M., Soto, C.E., Kariuki, B., and Zhou, J. 2003. Immortalized epithelial cells from human autosomal dominant polycystic kidney cysts. *Am. J. Physiol. Renal Physiol.* **285**:F397–F412.
41. Bernstein, J., and Gilbert-Barness, E. 1994. Congenital malformation of the kidney. In *Renal pathology.* B. Brenner, editor. J.B. Lippincott Co. Philadelphia, Pennsylvania, USA. 1366 pp.
42. Huan, Y., and van Adelsberg, J. 1999. Polycystin-1, the PKD1 gene product, is in a complex containing E-cadherin and the catenins. *J. Clin. Invest.* **104**:1459–1468.
43. Kim, H., Bae, Y., Jeong, W., Ahn, C., and Kang, S. 2004. Depletion of PKD1 by an antisense oligodeoxynucleotide induces premature G1/S-phase transition. *Eur. J. Hum. Genet.* **12**:433–440.
44. Gartel, A.L., and Tyner, A.L. 1999. Transcriptional regulation of the p21((WAF1, CIP1)) gene. *Exp. Cell Res.* **246**:280–289.
45. Thomson, R.B., et al. 2003. Histopathological analysis of renal cystic epithelia in the Pkd2WS25/- mouse model of ADPKD. *Am. J. Physiol. Renal Physiol.* **285**:F870–F880.
46. Woo, D. 1995. Apoptosis and loss of renal tissue in polycystic kidney diseases. *N. Engl. J. Med.* **333**:18–25.
47. Arnould, T., et al. 1998. The polycystic kidney disease 1 gene product mediates protein kinase C alpha-dependent and c-Jun N-terminal kinase-dependent activation of the transcription factor AP-1. *J. Biol. Chem.* **273**:6013–6018.
48. Wood, S.A., Allen, N.D., Rossant, J., Auerbach, A., and Nagy, A. 1993. Non-injection methods for the production of embryonic stem cell-embryo chimaeras. *Nature.* **365**:87–89.
49. Kojima, S., et al. 2001. Testicular germ cell apoptosis in Bcl6-deficient mice. *Development.* **128**:57–65.

ARTHRITIS & RHEUMATISM
Vol. 52, No. 9, September 2005, pp 2697–2707
DOI 10.1002/art.21258
© 2005, American College of Rheumatology

Butyrate Suppresses Tumor Necrosis Factor α Production by Regulating Specific Messenger RNA Degradation Mediated Through a *cis*-Acting AU-Rich Element

Jun Fukae, Yoshiharu Amasaki, Yumi Yamashita, Toshiyuki Bohgaki, Shinsuke Yasuda, Satoshi Jodo, Tatsuya Atsumi, and Takao Koike

Objective. **To study the capacity of butyrate to inhibit production of tumor necrosis factor α (TNFα) in macrophage-like synoviocytes (MLS) from patients with rheumatoid arthritis (RA), in human peripheral monocytes, and in murine RAW264.7 macrophages.**

Methods. **The concentrations of TNFα in culture supernatants of these cells were measured using enzyme-linked immunosorbent assay. The expression levels of various messenger RNAs (mRNA), such as those for TNFα, the mRNA-binding protein TIS11B, and luciferase, were measured using real-time quantitative polymerase chain reaction. The in vitro effects of butyrate on transcriptional regulation were evaluated by transfection with various reporter plasmids in RAW264.7 macrophages. The effects of TIS11B on TNFα expression were examined using an overexpression model of TIS11B in RAW264.7 cells.**

Results. **Butyrate suppressed TNFα protein and mRNA production in MLS and monocytes, but paradoxically enhanced transactivation of the TNFα promoter. Expression of the AU-rich element (ARE)–binding protein TIS11B was up-regulated by butyrate. Induction of TNFα mRNA by lipopolysaccharide was significantly inhibited when TIS11B was overexpressed. Butyrate facilitated the degradation of luciferase transcripts containing the 3′-untranslated region (3′-UTR) of TNFα, and this effect was dependent on the ARE in the 3′-UTR that is known to be involved in the regulation of mRNA degradation.**

Conclusion. **These results indicate that butyrate suppresses TNFα expression by facilitating mRNA degradation mediated through a *cis*-acting ARE. Butyrate has the ability to regulate TNFα at the mRNA level and is therefore a potential therapeutic drug for RA patients.**

Rheumatoid arthritis (RA) is a chronic inflammatory disease characterized by cartilage destruction and extracellular matrix degradation in multiple joints (1). The pathogenesis of RA is not clearly understood; however, tumor necrosis factor α (TNFα) is involved in its development, a conclusion which is supported by successful treatments with anti-TNFα reagents (2). The production of TNFα was found to be increased in rheumatoid synovium, followed by the induction of other proinflammatory cytokines, including interleukin-1β (IL-1β), IL-6, and IL-8, as well as matrix metalloproteinases involved in cartilage and bone destruction in RA (3–5). These cytokines are involved in synovial cell activation and proliferation, leading to generation of pannus (6).

Synovial tissue consists of heterogeneous immune and non–immune cell populations, including fibroblast-like synoviocytes, macrophage-like synoviocytes (MLS), lymphocytes, dendritic cells, and endothelial cells (7). Among these populations, MLS originating from bone marrow–derived monocytes are largely responsible, upon activation, for the production of TNFα protein (6). Monocytes can give rise to osteoclasts involved in rheumatoid bone destruction (8). The mech-

Supported by the Ministry of Education, Science, Technology, Sports, and Culture of Japan (grant 14570004) and by a research grant for study of the action of short chain fatty acids on cytokine gene regulation.

Jun Fukae, MD, PhD, Yoshiharu Amasaki, MD, PhD, Yumi Yamashita, PhD, Toshiyuki Bohgaki, MD, PhD, Shinsuke Yasuda, MD, PhD, Satoshi Jodo, MD, PhD, Tatsuya Atsumi, MD, PhD, Takao Koike, MD, PhD: Hokkaido University Graduate School of Medicine, Sapporo, Japan.

Address correspondence and reprint requests to Yoshiharu Amasaki, MD, Department of Medicine II, Hokkaido University Graduate School of Medicine, Kita-15, Nishi-7, Kita-ku, Sapporo 060-8638, Japan. E-mail: yamasaki@med.hokudai.ac.jp.

Submitted for publication December 6, 2004; accepted in revised form June 3, 2005.

anisms of MLS activation have been only partially understood. Macrophages express TNFα via activation of Toll-like receptor 4–NF-κB signaling, and this type of activation may be mimicked experimentally by administration of lipopolysaccharide (LPS) (9,10).

TNFα-mediated chronic inflammation has also been studied in inflammatory bowel diseases and in animal models of such diseases. In those studies, physiologic roles for short-chain fatty acids have been identified (11,12). Short-chain fatty acids are a natural product of colonic anaerobic fermentation of dietary fiber by luminal microflora. These are the preferred sources of energy for the normal colonic epithelial cell, and they can modulate a variety of fundamental cellular processes to induce cell-cycle arrest, differentiation, and apoptosis in transformed cells (13,14). These molecules, especially butyrate, have potent antiinflammatory effects and can modulate TNFα expression in colonic epithelial cells and in monocytes (15). It has also been shown that administration of butyrate suppresses experimental enteritis induced in mice by dextran sulfate sodium (16). Experiments in colonocytes revealed that butyrate down-regulates TNFα expression by modulating NF-κB–DNA binding activity (15), although the precise mechanism is not fully understood. In addition, butyrate is known to function as a histone deacetylase (HDA) inhibitor in cells, and it can induce alteration of the chromatin structure (17,18), although the effect of this activity on TNFα down-regulation is not yet understood. We investigated whether butyrate could suppress TNFα production in activated synovial cells and macrophages, in order to evaluate short-chain fatty acids as a potential investigational new treatment for chronic inflammation in RA.

MATERIALS AND METHODS

Preparation of primary synoviocytes and culture. Primary synoviocytes were obtained from surgically resected synovial tissue from Japanese patients with RA. Informed consent was obtained from each patient. Tissue specimens were minced and dissociated in Hanks' balanced salt solution (Invitrogen, Carlsbad, CA) containing 5 mg/ml type I collagenase (Sigma, St. Louis, MO) and 0.15 mg/ml DNase I (Sigma) for 2 hours at 37°C. Samples were then passed through a metal mesh and a nylon mesh, each with a 100-μm pore size. Cells were collected by centrifugation and resuspended at 0.5×10^6/ml in Iscove's modified Dulbecco's medium (Invitrogen) containing 10% heat-inactivated fetal bovine serum (FBS) and antibiotics. The resulting synoviocytes were cultured in a 6-well tissue culture plate (Becton Dickinson, Mountain View, CA) at 37°C in a humidified atmosphere with 5% CO_2 for 24–48 hours. Our primarily rheumatoid synoviocyte cultures contained ~10–35% of a CD14-positive subpopulation as assessed by fluorescence-activated cell sorting (FACS Calibur system; Becton Dickinson) (data not shown). The proportion of CD14-positive rheumatoid synoviocytes varied depending on the patient's background, such as duration or activity of the disease and treatment. Before the stimulation assay, nonadherent cells were removed by washing twice with phosphate buffered saline (PBS).

Cell culture and stimulation. Human monocytes were enriched from whole blood obtained from healthy Japanese volunteers. The mononuclear cell fraction was prepared by density-gradient centrifugation over Ficoll-Paque (Amersham Biosciences, Uppsala, Sweden), followed by plating in culture medium at 37°C for 1 hour in a humidified incubator to obtain the adherent cells. After washing the cells twice with PBS, adherent cells were resuspended in RPMI 1640 medium (Invitrogen) containing 10% heat-inactivated FBS and antibiotics, then counted and diluted to 0.5×10^6/ml. Cells were processed for the stimulation assay on the same day that the blood was collected. Purity of CD14-positive cells was 80–90% as assessed by fluorescence-activated cell sorting (data not shown). The murine macrophage cell line RAW264.7 (no. TIB-71; American Type Culture Collection, Rockville, MD) was grown in Dulbecco's modified Eagle's medium (DMEM; Invitrogen) containing 10% heat-inactivated FBS and antibiotics at 37°C in a humidified atmosphere with 5% CO_2 (19). Cells were resuspended at 0.25×10^6/ml, then 2 ml/well of the cell suspension was transferred to 6-well tissue culture plates, followed by 24 hours of culture before stimulation. After preincubation, cells were stimulated with LPS (no. L4391; Sigma) or were used without stimulation. In some experiments, various concentrations of sodium butyrate (Sigma) were included in the culture. Where indicated, actinomycin D (Sigma) was also included in the culture to restrict transcriptional events.

RNA preparation and real-time quantitative polymerase chain reaction (PCR) analysis. Total RNA was obtained by using TRIzol RNA Reagent (Invitrogen) according to the manufacturer's instructions. In some experiments, total RNA was extracted from transfected cells using the Concert Cytoplasmic RNA Reagent (Invitrogen) in combination with DNase I Amplification Grade (Invitrogen) to eliminate residual plasmid DNA. RNA samples were reverse-transcribed using oligo(dT) primers and ReverTra Ace (Toyobo, Osaka, Japan) according to the manufacturer's instructions. Real-time quantitative PCR analyses were performed using 100 n*M* TaqMan probe and 200 n*M* forward and reverse primers in a final volume of 30 μl using 2×PCR reagent (Applied Biosystems, Chiba, Japan) in an ABI PRISM 7000 Sequence Detection System instrument (Applied Biosystems) based on dual-labeled fluorogenic probe technology (20).

The following forward and reverse primers and TaqMan probes, designed by Primer Express software (Applied Biosystems), were used for analyses: mouse TNFα, forward primer 5′-CAGACCCTCACACTCAGATCATCT-3′, reverse primer 5′-GCACCACTAGTTGGTTGTCTTTGA-3′, TaqMan probe 5′-CAAGCCTGTAGCCCACGTCGTAGCA-3′; mouse TIS11B, forward primer 5′-TTGTTGGTAGCTTCTGGCTTGA-3′, reverse primer 5′-GGCATCTACTGACAAAAGATGGAA-3′, TaqMan probe 5′-TCCATTTCATAGCCCACTTAACCACGCA-3′; luciferase, forward primer 5′-TGACCGCCTGAAGTCTCTGA-3′, reverse primer 5′-

ACACCTGCGTCGAAGATGTTG-3′, TaqMan probe 5′-CCGCTGAATTGGAATCCATCTTGCTC-3′; AU-rich element (ARE) mutation, forward primer 5′-ATGCACAG-CCTTCCTCACAG-3′, reverse primer 5′-CCCGGCCT-TCCAAATAAATAC-3′, minor groove binder (MGB) TaqMan probe 5′-TATCCATTATCCATCCATTATCCATC-3′. The first 3 TaqMan probes were labeled on the 5′ end with FAM reporter dye and on the 3′ end with TAMRA quencher dye; the ARE mutation MGB TaqMan probe was labeled on the 5′ end with FAM reporter dye and on the 3′ end with conjugated MGB.

To measure the gene copy number of the various transcripts, the purified artificial gene product containing an amplification sequence was serially diluted to achieve a standard curve. Data for each messenger RNA (mRNA) quantity were normalized based on the mRNA copy number of GAPDH obtained using the TaqMan rodent GAPDH control reagents (Applied Biosystems).

Enzyme-linked immunosorbent assay (ELISA). The concentrations of human and mouse TNFα proteins were determined using specific sandwich ELISA kits (no. 656227 from Cosmo Bio [Tokyo, Japan] and no. 10019 from Genzyme [Cambridge, MA], respectively) according to the manufacturers' instructions.

Plasmid construction. The luciferase reporter plasmids pNFκB-Luc and pGL3-BASIC were purchased from Stratagene (La Jolla, CA) and Promega (Madison, WI), respectively. Murine genomic DNA extracted from a normal C57BL/6 mouse using a standard protocol (21) was used for amplification of a genomic DNA fragment of the mouse TNFα gene. A 0.9-kb DNA fragment corresponding to the 5′-untranslated region (5′-UTR) of the mouse TNFα gene was PCR-amplified with the sense and antisense primers 5′-CTC-AAGCTTATCAGAGTGAAAGGAGAAGGC-3′ and 5′-CTCAAGCTTAGTGAAAGGGACAGAACCTGC-3′, respectively. The product was inserted into the *Hind* III cloning site of pGL3-BASIC and designated pGL-mTNFα. The 0.8-kb 3′-UTR of the mouse TNFα gene was similarly amplified using PCR, and the *Xba* I and *Bam* HI restriction sites were introduced with the PCR primers 5′-TCTAGAGGGAATGGG-TGTTCATCC-3′ and 5′-GGATCCCATGCCCCAGGGCAAA-3′, respectively. The resulting DNA fragment was used to replace the 3′-UTR of the pGL-mTNFα, and the resulting plasmid was designated pGL-mTNFα-UTR.

A pGL-CMV-UTR plasmid, in which the luciferase gene was constitutively expressed under the control of the cytomegalovirus (CMV) promoter, was generated by replacing the *Hind* III fragment corresponding to the TNFα promoter region in the pGL-mTNFα-UTR vector with a DNA fragment containing the CMV promoter sequences from pFLAG-CMV-2 (Sigma). In addition, the AT repeat (ARE) in pGL-CMV-UTR corresponding to the TNFα 3′-UTR sequence (+1299 to +1332) was mutated to yield an ARE mutation plasmid (pGL-CMV-UTR/mARE) using standard recombinant techniques and the mutagenic oligonucleotide 5′-ACAGCCTTCCTCACAGAGCCAGCCCCCCTCTATT-TATATTTGCACTTATTATCCATTATCCATCCATTAT-CCATCCATTTGCTTATGAATGTATTTATTTGGAAG-GCCG-3′. The sequences of all the DNA fragments obtained by PCR amplification were confirmed by DNA sequencing and completely matched the reported mouse TNFα genomic sequence (GenBank accession no. Y00467) (22).

A mammalian expression plasmid, pFLAG-TIS11B, that encodes mouse TIS11B complementary DNA (cDNA) (23) was generated by introducing a mouse full-length TIS11B cDNA fragment into the pFLAG-CMV-2 plasmid (Sigma). The TIS11B cDNA fragment was obtained by PCR amplification of cDNA from RAW264.7 cells and the specific sense and antisense primers 5′-GAATTCGATGACCACCACCCTCGT-3′ and 5′-TCTAGAGGAGAGGTGAAGGAGGCATG-3′, respectively. After subcloning into pCR-blunt and confirmation by DNA sequencing, the 1.2-kb fragment corresponding to the TIS11B cDNA (GenBank accession no. BC016621) was excised and ligated into pFLAG-CMV-2 at the *Xba* I and *Eco* RI cloning sites.

Transfection and luciferase assay. RAW264.7 cells (0.25×10^5) were transferred to 8-cm tissue culture plates (Becton Dickinson) and incubated for 24 hours to 70% confluence. Transfections were achieved using Transfectam reagent (Promega), according to the manufacturer's instructions, with the plasmids described above. Plasmid DNA (10 μg) was mixed with 20 μl of Transfectam reagent in 3 ml of FBS-free DMEM and transferred to the plates. After 2 hours of incubation, complete culture medium was added to the cells, followed by further incubation to semiconfluence. The transfection efficiency in the current protocol was ~5% when cells transfected with green fluorescent protein–expressing plasmid were analyzed by fluorescence-activated cell sorting (data not shown). Transfected cells were collected and distributed into new 6-well tissue culture plates (Becton Dickinson) before the stimulation assay. This step was performed to equalize the number of transfected cells and eliminate any differences in transfection efficiency between plates.

Where indicated, the luciferase assay was carried out according to the procedure described previously with minimal modifications (24). Briefly, RAW264.7 cells were transfected with various reporter plasmids as described above. After incubation and stimulation, cells were lysed using lysis buffer (Promega). Cell lysates were stored at −80°C until the luciferase assay was performed. The protein content of each sample was determined using a protein assay reagent (Bio-Rad, Hercules, CA), and the luciferase activities of the samples were normalized according to the protein content of the samples. Data are reported as relative luciferase units.

Cell proliferation assay. In order to exclude the possibility that butyrate directly affects cell viability, a proliferation assay was performed using MTS (3-(4,5-dimethylthiazol-2-yl)-5-(3-carboxymethoxyphenyl)-2-(4-sulfophenyl)-2H-tetrazolium) tetrazolium assay (Cell Titer96 AQueous One Solution Cell Proliferation Assay; Promega). RAW264.7 cells (0.25×10^5) were transferred into microtiter-plate wells in 100 μl of DMEM containing various concentrations of butyrate, then MTS reagent was added to the wells. Optical density was read using a microplate autoreader (Microplate Reader Model 3550; Bio-Rad) at a wavelength of 490 nm after addition of MTS reagent.

Statistical analysis. Statistical analyses were calculated by Student's *t*-test with the use of the Excel program (Microsoft, Redmond, WA).

RESULTS

Suppression by butyrate of TNFα protein production in cultured primary synoviocytes. We first analyzed the effect of butyrate on TNFα production in rheumatoid synoviocytes during stimulation with LPS. When primary synoviocytes were stimulated with LPS, significant amounts of TNFα protein were detected in the culture supernatants (Figure 1A). Addition of butyrate to the culture medium led to a significant, dose-dependent decrease in LPS-stimulated TNFα production. MLS, major producers of TNFα in the rheumatoid inflammatory synovium, play an important role in the initiation of synovitis and bone destruction (25). We paid attention to the subpopulation of monocyte/macrophages, and thus we repeated the experiments on the effect of butyrate on TNFα production both by peripheral monocytes and by the macrophage cell line RAW264.7. Human peripheral monocytes and RAW264.7 cells both secreted significant amounts of TNFα upon LPS stimulation (Figures 1B and C). As was the case in the primary cell culture, there was a significant decrease in LPS-stimulated TNFα secretion with increasing butyrate concentrations in the medium. In all experiments, similar GAPDH mRNA expression levels were confirmed in each cell preparation after treatment with LPS/butyrate (data not shown).

RAW264.7 cells were exposed to various concentrations of butyrate, and MTS tetrazolium assay was performed to assess cell proliferation. The results revealed that butyrate had no significant effect on cell proliferation (Figure 2B).

Suppression by butyrate of TNFα expression at the mRNA level in monocytes and in the macrophage cell line RAW264.7. To determine how butyrate regulates TNFα production in monocytes, we next examined the effect of butyrate on TNFα mRNA expression. We performed semiquantitative reverse transcriptase (RT)–PCR analysis using specific primers for initial screening and found that butyrate suppressed TNFα mRNA induction in response to stimulation with LPS in human monocytes (data not shown). Butyrate also suppressed LPS-stimulated TNFα production in RAW264.7 cells in a dose-dependent manner, confirmed by real-time quantitative PCR (Figure 2A). The macrophage cell line RAW264.7 is responsive to butyrate; therefore, we used the RAW264.7 cells as an appropriate system for transfection assay.

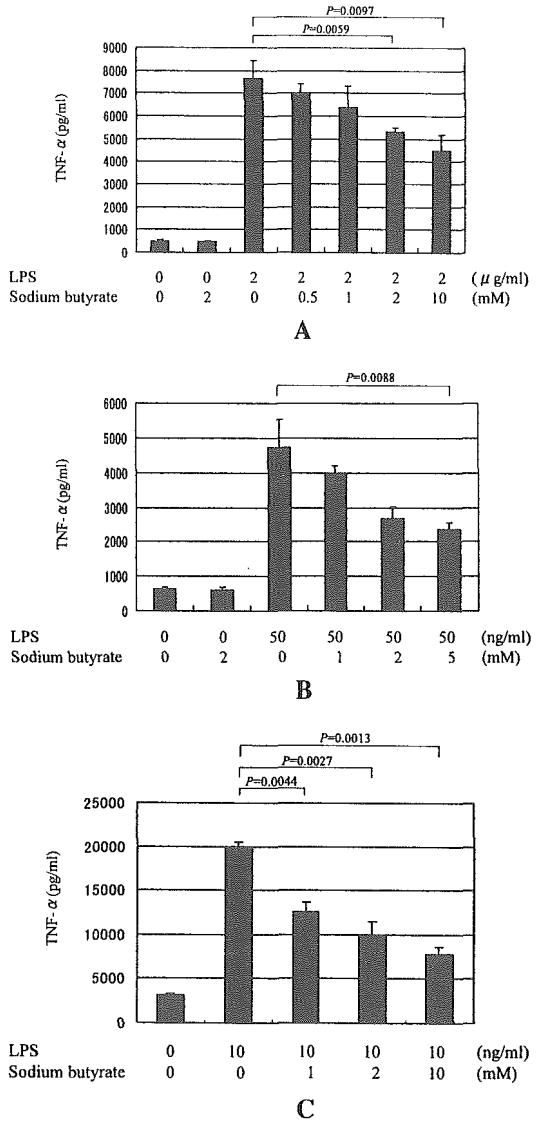

Figure 1. Effects of butyrate on tumor necrosis factor α (TNFα) protein secretion by synoviocytes and monocytes. An enzyme-linked immunosorbent assay (ELISA) specific for human TNFα protein was used to determine levels of TNFα in **A,** culture supernatants of primary synoviocytes (obtained from patients with rheumatoid arthritis) not stimulated with lipopolysaccharide (LPS) or stimulated with 2 μg/ml LPS for 6 hours in the presence or absence of sodium butyrate, and **B,** human peripheral blood monocytes (obtained from healthy donors) not stimulated with LPS or stimulated with 50 ng/ml LPS for 4 hours in the presence or absence of sodium butyrate. **C,** Levels of mouse TNFα were measured in culture supernatants from RAW264.7 cells not stimulated with LPS or stimulated with 10 ng/ml LPS for 6 hours in the presence or absence of sodium butyrate, using an ELISA specific for mouse TNFα. Experiments in **A, B,** and **C** were repeated 15, 9, and 6 independent times, respectively, and representative results are shown. Values are the mean and SEM.

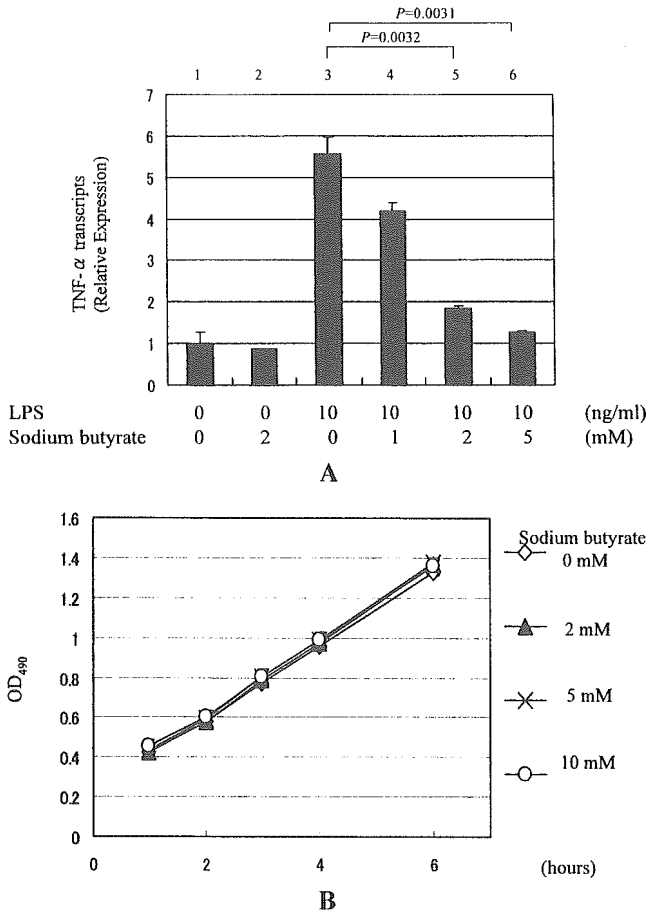

Figure 2. Effects of butyrate on TNFα mRNA expression and cell proliferation in RAW264.7 cells. **A,** Real-time quantitative polymerase chain reaction (PCR) (described in Materials and Methods) was used to estimate TNFα expression in RAW264.7 cells not stimulated with LPS (lanes 1 and 2) or stimulated with 10 ng/ml LPS (lanes 3–6) in the presence (lanes 2 and 4–6) or absence (lanes 1 and 3) of sodium butyrate for 2 hours. The amount of TNFα cDNA transcripts is displayed as a relative value obtained by dividing the value for TNFα transcripts by the value for GAPDH cDNA transcripts. Real-time quantitative PCR data were obtained from triplicate transwells and are representative of 3 independent experiments. Values are the mean and SEM. **B,** Cell proliferation assay (described in Materials and Methods) was used to examine the toxicity of butyrate on RAW264.7 cells. Cells were treated with various concentrations of butyrate (0, 2, 5, and 10 m*M*), and the optical density (OD) was read at a wavelength of 490 nm serially at 1-, 2-, 3-, 4-, and 6-hour time points. Data were obtained from triplicate transwells. Values are the mean ± SEM of 3 independent experiments. See Figure 1 for other definitions.

No suppression by butyrate of transcriptional activity driven through the TNFα promoter. To test whether butyrate could affect TNFα mRNA expression via transcriptional repression, RAW264.7 cells were transfected with reporter plasmids containing the consensus NF-κB binding sequence or the full-length TNFα promoter sequence. When cells were transfected with pNFκB-Luc or pGL-mTNFα, however, butyrate did not suppress the transcriptional activities (Figures 3A and B). Instead, butyrate showed a dose-dependent enhancement of transactivation, which was inconsistent with its effects on the mRNA and protein expression of TNFα. These results indicate that butyrate regulates TNFα mRNA levels via a mechanism other than transcriptional repression in RAW264.7 cells.

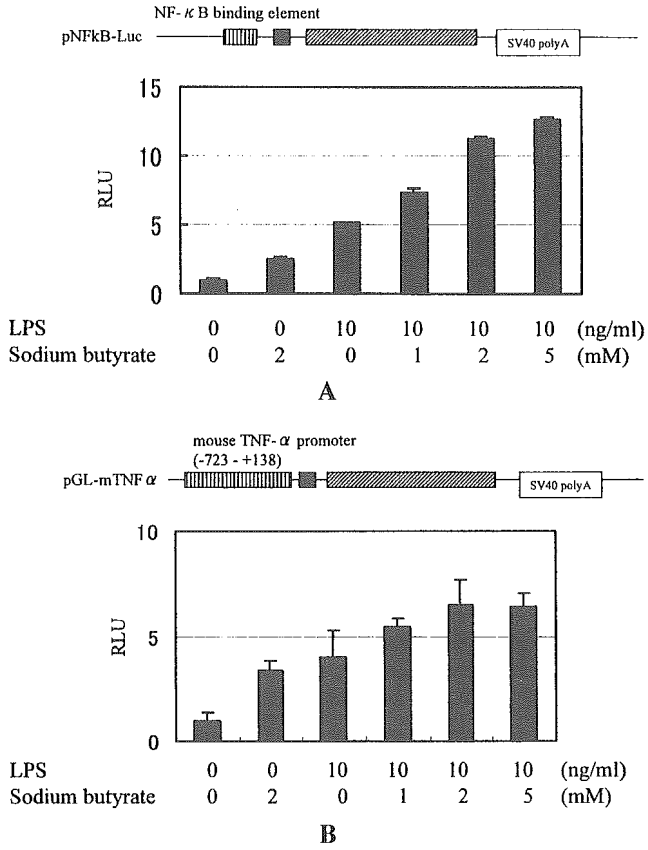

Figure 3. Effect of butyrate on TNFα promoter–related transcriptional activities. RAW264.7 cells were transfected with various types of luciferase reporter plasmids (see Materials and Methods for description of methods of transfection and luciferase assay). Forty-eight hours after transfection, cells were stimulated with 10 ng/ml LPS in the absence or presence of sodium butyrate (1, 2, or 5 m*M*) for 6 hours. The luciferase activities in cell lysates were measured and normalized using the protein concentration in each sample. **A,** Transcriptional activity of cells transfected with pNFκB-Luc. **B,** Transcriptional activity of cells transfected with pGL-mTNFα. Data shown in **A** and **B** were obtained from triplicate transwells and are representative of 6 independent experiments. Values are the mean and SEM. SV40 polyA = simian virus 40 late poly(A) signal; RLU = relative luciferase units (see Figure 1 for other definitions).

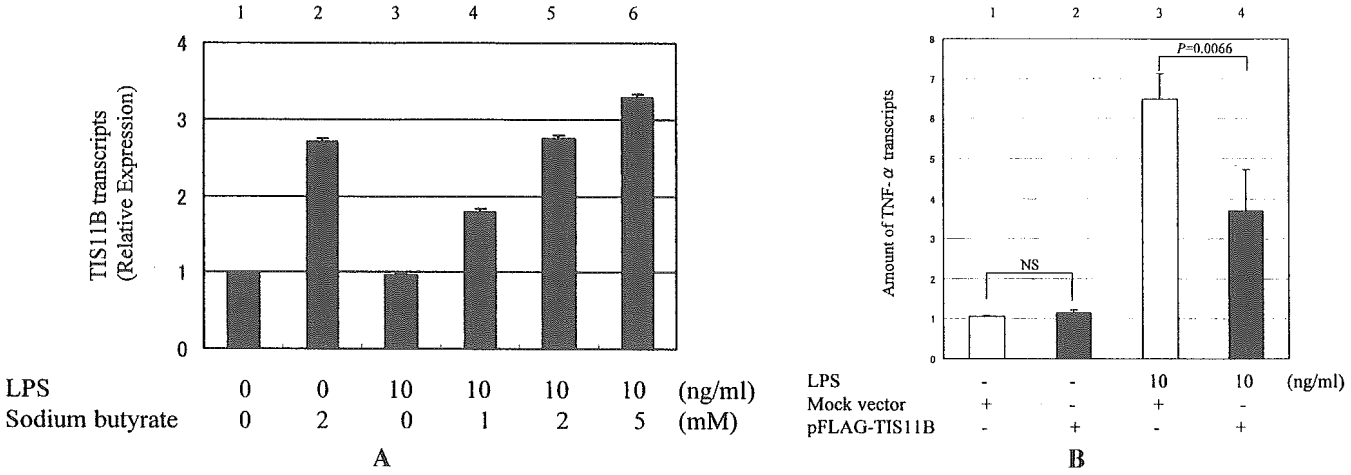

Figure 4. Expression of the tristetraprolin (TTP) family of genes in RAW264.7 cells upon treatment with butyrate. **A,** Expression of mRNA for TIS11B (a representative member of the TTP family of proteins) in RAW264.7 cells upon treatment with butyrate. RAW264.7 cells were not stimulated with LPS or were stimulated with 10 ng/ml LPS (lanes 3–6) in the presence (lanes 2 and 4–6) or absence (lanes 1 and 3) of butyrate. After 1 hour of stimulation, total RNA was obtained, followed by real-time quantitative polymerase chain reaction (PCR) for TIS11B. The amount of TIS11B cDNA transcripts is displayed as a relative value obtained by dividing the value for TIS11B transcripts by the value for GAPDH cDNA transcripts. Real-time quantitative PCR data were obtained from triplicate transwells and are representative of 3 independent experiments. Values are the mean and SEM. **B,** Effect of TIS11B on expression levels of TNFα mRNA in RAW264.7 cells stimulated with LPS. RAW264.7 cells were transfected with the TIS11B expression vector, pFLAG-TIS11B (solid bars) or with the control pFLAG empty (mock) vector (open bars). Forty-eight hours after transfection, cells were stimulated with 10 ng/ml LPS (lanes 3 and 4); total RNA was obtained after 2 hours of stimulation. The amount of TNFα cDNA transcripts was determined using real-time quantitative PCR. Data are schematically displayed as a relative value obtained by dividing the value for TNFα transcripts by the value for GAPDH cDNA transcripts. Real-time quantitative PCR data were obtained from triplicate transwells and are representative of 3 independent experiments. Values are the mean and SEM. NS = not significant (see Figure 1 for other definitions).

TIS11B as a candidate molecule for butyrate-mediated inhibition of TNFα mRNA expression. TNFα gene expression involves posttranscriptional regulation, including the ARE in the 3′-UTR that is thought to play a critical role in the regulatory mechanism (26). AREs are found in multiple cytokine genes including TNFα, and the *cis*-regulatory effects of these elements are mediated by several polypeptides that can bind AREs. Tristetraprolin (TTP) is an ARE-binding protein that facilitates TNFα mRNA degradation, and TIS11B and TIS11D are representative members of the TTP family of proteins that are also capable of interacting with AREs. We hypothesized that the effects of butyrate were related to the posttranscriptional regulation mediated through the AREs and ARE-binding proteins. To search for the butyrate-mediated induction of ARE-binding proteins, we first used semiquantitative RT-PCR to screen for the expression of TTP family proteins such as TTP, TIS11B, and TIS11D in RAW264.7 cells treated with butyrate. Among the factors examined, butyrate induced only TIS11B mRNA but neither TTP mRNA nor TIS11D mRNA (data not shown). Real-time quantitative PCR revealed that butyrate induced TIS11B mRNA in a dose-dependent manner (Figure 4A).

We determined that TIS11B had a suppressive effect on levels of TNFα mRNA. RAW264.7 cells were transfected with TIS11B expression plasmid or with a control mock vector, then stimulated with LPS. The expression level of TNFα mRNA decreased significantly in RAW264.7 cells transfected with TIS11B expression plasmid (Figure 4B). These results suggested that butyrate down-regulated levels of TNFα mRNA via binding of TIS11B to an ARE.

Facilitation by butyrate of mRNA degradation via the function of an ARE in the TNFα 3′-UTR. We next studied whether the inhibitory effects of butyrate on TNFα specifically depended on an ARE. To determine whether butyrate affects the amounts of gene transcripts carrying the TNFα 3′-UTR, we designed a real-time TaqMan RT-PCR–based quantitative assay that detects mRNA turnover (Figure 5). RAW264.7 cells were transfected with pGL-CMV-UTR reporter plasmid and treated with actinomycin D to repress generation of newly transcribed mRNA. To equalize the difference in transfection efficiency between plates, all transfected

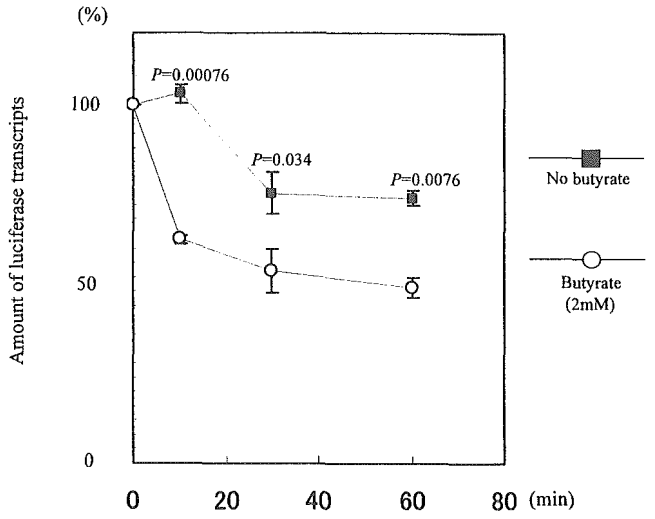

Figure 5. Effect of butyrate on the turnover of luciferase mRNA containing a tumor necrosis factor α 3′-untranslated region. RAW264.7 cells were transfected with pGL-CMV-UTR (see Materials and Methods). After no treatment or pretreatment with butyrate (2 m*M*) for 2 hours, cells were placed in culture medium containing actinomycin D (10 μg/ml) to halt transcription. Cells were then harvested serially at 0-, 10-, 30-, and 60-minute time points, and total RNA was extracted. After extensive treatment with RNase-free DNase I to digest the plasmid vector DNA, total RNA samples were reverse-transcribed for real-time quantitative polymerase chain reaction using primers specific for the luciferase gene product (described in Materials and Methods). The amount of luciferase cDNA transcripts is displayed as a relative value obtained by dividing the value for luciferase transcripts by the value for GAPDH cDNA transcripts. The datum at the 0-minute time point (for luciferase/GAPDH) was assigned a value of 100%, and other data are shown relative to this value. Values are the mean ± SEM of 3 independent experiments.

cells were collected and distributed into new plates before butyrate treatment. The time course of decrease of mRNA levels was in direct proportion to the rate of degradation. The amount of cDNA transcripts containing the 3′-UTR was serially quantified by real-time PCR. We observed a significant decrease in cDNA transcripts derived from pGL-CMV-UTR in cells treated with butyrate, both at the 10-minute time point and thereafter (Figure 5). This suggested that butyrate facilitated the degradation of mRNA transcripts of TNFα carrying the 3′-UTR sequence.

In various cytokine genes, including TNFα, an ARE in the 3′-UTR has been shown to affect stability of the gene transcripts (26). To test whether the inhibitory effects of butyrate on TNFα are mediated by the action of this *cis* ARE, we generated pGL-CMV-UTR/mARE containing a mutated ARE from pGL-CMV-UTR (Figure 6A). The amounts of transcripts derived from these plasmids were quantified and compared using RAW264.7 cells and the TaqMan PCR method. In this assay, total amounts of transcripts derived from mixed plasmids were determined by reactions using a luciferase TaqMan probe, and, at the same time, amounts of transcripts carrying the ARE mutation derived from these mixed plasmids were determined using an ARE mutation MGB TaqMan probe (Figure 6A). The quantification of these 2 transcripts was made possible by using a common gene standard, R-luc-AU, that contained both the mutated ARE and part of the common luciferase open reading frame sequence, and changes in the expression of these 2 transcripts were described as a ratio and calculated as follows: transcripts with mutated ARE:transcripts with intact ARE = (M/G):([A − M]/G) = M:(A − M), where A is the total amount of luciferase transcripts, M is the amount of transcripts with mutated ARE, and G is the internal control GAPDH.

As shown in Figure 6B, the amount of transcripts carrying mutated ARE and the amount carrying intact ARE were almost identical at the time point at which actinomycin D had stopped the transcription, when cells were treated (or not treated) with butyrate. It was shown that the relative amount of transcripts carrying a mutated ARE increased significantly during the time course. Thus, transcripts carrying the mutated ARE were more stable than those carrying intact ARE, and butyrate's ability to facilitate the degradation of transcripts was lost when the ARE was mutated. This indicates that the suppressive effect of butyrate on TNFα expression is mediated through the specific ARE in the 3′-UTR of the TNFα transcript.

DISCUSSION

In this report, we have shown that butyrate strongly down-regulated the production of TNFα in primary synoviocytes, peripheral monocytes, and murine RAW264.7 macrophages at the mRNA level. Our results also indicated that butyrate induced an ARE-binding protein, TIS11B, that could facilitate TNFα mRNA degradation. The collective data led us to believe that the down-regulation of TNFα expression by butyrate was mediated through the TIS11B protein that bound to a specific ARE and facilitated mRNA degradation.

TNFα is a key cytokine in the pathogenesis of RA. Therefore, inhibition of the action of TNFα may improve the clinical course of patients with RA. Biologic agents designed to interfere with the action of TNFα

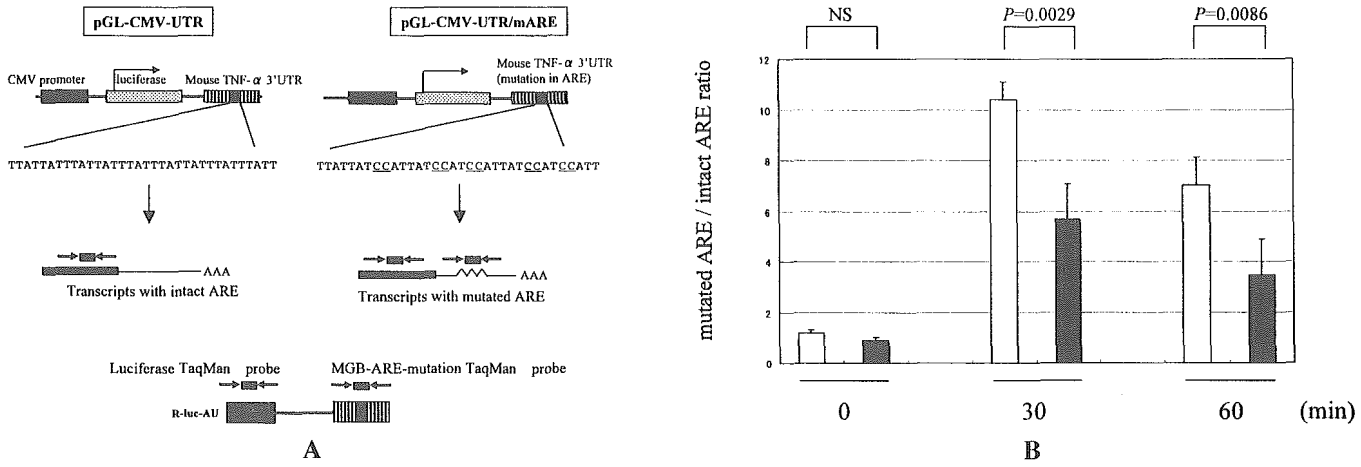

Figure 6. Effects of mutations in AU-rich elements (AREs) on the ability of butyrate to modify mRNA turnover. **A**, Schematic diagram of the plasmids, primers, and TaqMan probes that were used in these experiments. The plasmid pGL-CMV-UTR/mARE was derived by mutating the ARE of the 3′-untranslated region (3′-UTR) of the plasmid pGL-CMV-UTR (see Materials and Methods). To measure the gene copy number of the transcripts derived from pGL-CMV-UTR and pGL-CMV-UTR/mARE, the artificial DNA fragment R-luc-AU was generated from pGL-CMV-UTR/mARE by polymerase chain reaction (PCR) amplification. The R-luc-AU fragment, which contained both the ARE mutation and part of the common luciferase open reading frame sequence, was used to produce both the standard curve for the total luciferase transcripts and the curve for transcripts containing the ARE mutation. **B**, Quantitative PCR analysis of the reporter gene products carrying intact or mutated ARE. RAW264.7 cells were transfected with a 50:50 mixture of pGL-CMV-UTR/mARE and pGL-CMV-UTR. Cells were then not treated (solid bars) or pretreated with 5 m*M* sodium butyrate for 2 hours (open bars) and placed in culture medium containing actinomycin D (10 μg/ml) to halt transcription. Cells were then harvested serially at 0-, 30-, and 60-minute time points, and total RNA was extracted. Degradation of plasmid DNA and subsequent cDNA synthesis were carried out using the same method described in Figure 5. Real-time quantitative PCR analyses were done using a TaqMan probe, with specific forward and reverse primers (see Materials and Methods). The amounts of total luciferase cDNA transcripts and transcripts with mutated ARE were determined, and the y-axis shows the ratio of cDNA transcripts with mutated ARE to cDNA transcripts with intact ARE. Data were obtained from triplicate transwells and are representative of 5 independent experiments. Values are the mean and SEM. CMV = cytomegalovirus; TNFα = tumor necrosis factor α; MGB = minor groove binder; NS = not significant.

have been approved for the treatment of RA, and they provide dramatic efficacy for the affected patients. However, the disadvantages of biologic agents, such as their high cost, their instability, the difficulty of producing them, and the immune reaction of the host toward them, remain to be addressed. Therefore, new chemical agents that down-regulate TNFα production have been researched extensively. Our current findings may provide a framework for the therapeutic down-regulation of TNFα production by butyrate or its analogs.

Butyrate facilitated the degradation of luciferase transcripts when the TNFα 3′-UTR cDNA sequence was included in the reporter construct. This effect appeared to be dependent on an ARE, since a mutation in the ARE in the reporter plasmids resulted in the loss of the butyrate-induced changes in the transcript turnover. Thus, butyrate could down-regulate TNFα mRNA expression by facilitating TNFα mRNA degradation through a mechanism that was dependent on the specific ARE.

AREs are several repetitive sequences of AUUUA or UUAUUUAUU present in the 3′-UTRs of various mRNA. The AREs are clustered into several categories and have been identified in a panel of genes other than TNFα (27–30). These genes largely encode proteins that regulate cellular growth and the body's response to exogenous agents such as microbes and inflammatory and environmental stimuli. The mRNA containing AREs are commonly short lived, rapidly expressed in response to stimuli, and rapidly degraded once their critical role in gene regulation ceases.

To date, several ARE-binding proteins have been reported that can stabilize or destabilize the target mRNA by binding competitively to their AREs. TTP (also known as TIS11, Nup475, and G0S24) is one of these ARE-binding proteins, and it has been characterized as a critical factor that controls TNFα mRNA turnover (31). Interestingly, genetically manipulated mice that lack TTP showed an abundance of endogenous TNFα production, an RA-like arthritis, and autoimmunity, presumably mediated by an excess of TNFα (32–34). TTP-related proteins, designated TIS11B and TIS11D, are structurally similar to TTP in their zinc-finger motifs, and they share functions with TTP, al-

though their unique functions have yet to be characterized (35). These TTP-related proteins are rapidly expressed in response to 12-*O*-tetradecanoylphorbol-13-acetate and other diverse stimuli in various types of eukaryotic cells (23,36). The expression of these proteins differs depending on the circumstances, hence they may have their own roles in controlling mRNA turnover under different circumstances (37). Among these proteins, TTP is induced by TNFα, suggesting that TTP may function as a feedback regulator of TNFα gene expression (31,38). Notably, a TIS11B homolog expressed rapidly in response to butyrate has also been discovered in human cells and characterized as butyrate response factor 1 (BRF1) (39).

Consistently, butyrate rapidly induced the expression of TIS11B in RAW264.7 cells (Figure 4A). In addition, the induction of TNFα mRNA by LPS stimulation was strongly inhibited when TIS11B was overexpressed in these cells (Figure 4B). Stoecklin et al identified BRF1 as a regulator of ARE-dependent mRNA decay, and also showed that BRF1 can bind directly to ARE and promote the degradation of ARE-containing mRNA (40). Thus, we postulated a model whereby butyrate induced the expression of TIS11B/BRF1, followed by the binding of this ARE-binding protein to the ARE, thus facilitating TNFα mRNA degradation. Our cDNA microarray (GeneNavigator cDNA Array System; Toyobo) revealed that butyrate suppressed expression of mRNA containing AREs in their 3′-UTRs (e.g., mRNA for IL-1β, IL-15, and granulocyte–macrophage colony-stimulating factor) (data not shown). This result further supported the relevance of our hypothesis.

TIS11B has a unique character that facilitates TNFα mRNA degradation; therefore, analyzing the regulation of this molecule would provide a novel approach to the control of TNFα production. TNFα expression is activated mainly by the transcription factor NF-κB and by the MAP kinase (MAPK) pathways (the ERK, JNK, and p38 MAPK pathways). Recent studies have shown that the p38 MAPK pathway in particular plays an important role in posttranscriptional regulation that leads to mRNA stabilization (41). The p38 MAPK pathway also strongly induces and activates TTP, which down-regulates TNFα (42–45). Those studies suggested that the p38 MAPK pathway may play a crucial role in regulating the expression of TNFα (involving a TTP-dependent mechanism); however, the precise mechanism is not completely understood, and less is known about the relationship between TIS11B and the p38 MAPK pathway. Since butyrate induced TIS11B expression and has been shown to affect the p38 MAPK pathway (46), it may be that butyrate influences TIS11B expression through the p38 MAPK pathway. Analysis of the relationship between TIS11B and the p38 MAPK pathway would be important for understanding the effect of butyrate.

The effects of butyrate on TNFα gene expression, other than those involving TIS11B- and ARE-dependent mechanisms, also need to be addressed. In previous studies, it was shown that butyrate can inhibit the binding of NF-κB to DNA (12,15,47). In contrast, in the reporter gene assays, butyrate enhanced the transcriptional activity driven by NF-κB sites and the TNFα promoter in a dose-dependent manner (Figures 3A and B). This phenomenon may be explained in part by the HDA-inhibitory effects of butyrate. Butyrate strongly inhibits HDA activity in cells, and it can cause hyperacetylation of nucleotides and thereby nonspecifically enhance transcriptional activity (18,48,49). As in the case of genomic DNA, transfected plasmid DNA has been shown to be assembled with histones to form a "minichromosome" that is sensitive to histone hyperacetylation (50). Thus, butyrate can function as a nonspecific transcriptional enhancer for transfected plasmid DNA; hence, cotransfection with an internal control was not informative in the current experiments.

Analysis of the regulation of TNFα by butyrate provides information for a novel approach to the treatment of patients with RA. Further investigation of the regulation of TIS11B expression, including study of its gene promoter, promises to pave the way for therapeutic approaches that address ARE-dependent cytokine gene regulation.

ACKNOWLEDGMENTS

We thank Ms Akiko Hirano and Ms Miki Aoto for technical assistance.

REFERENCES

1. Feldmann M, Brennan FM, Maini RN. Rheumatoid arthritis. Cell 1996;85:307–10.
2. Daniel CL, Moreland LW. Infliximab: additional safety data from an open label study. J Rheumatol 2002;29:647–9.
3. MacNaul KL, Chartrain N, Lark M, Tocci MJ, Hutchinson NI. Discoordinate expression of stromelysin, collagenase, and tissue inhibitor of metalloproteinases-1 in rheumatoid human synovial fibroblasts: synergistic effects of interleukin-1 and tumor necrosis factor-α on stromelysin expression. J Biol Chem 1990;265: 17238–45.
4. Chin JE, Winterrowd GE, Krzesicki RF, Sanders ME. Role of cytokines in inflammatory synovitis: the coordinate regulation of